博士論文

Capacity curve derivation using Wavelet Transform Method for building damage evaluation with limited number of accelerometers

（少数の加速度計を用いた高層建物の Wavelet 変換による性能曲線算出法に関する研究）

Pan Haoran

潘 浩然

Abstract

Structural health monitoring (SHM) has received increasing attention in recent decades and has found global success in applications ranging from long-span bridges to super-tall buildings. An SHM system offers a rapid and quantitative way to evaluate the safety of the structure using the response data from instrumented sensors. This merit could be helpful in quake-hit regions, where post-earthquake damage evaluations for buildings are generally conducted through time-consuming and subjective visual inspections by engineers. Several vibration-based methods have been developed to evaluate the damage condition after an earthquake, such as methods based on the change of modal parameters, e.g., natural frequencies, damping ratios, and mode shape; and methods based on tracking the hysteretic behaviors of the structures. Among other methods, the capacity curve, which is considered to be the fundamental mode relationship between mass-normalized roof displacement and base shear, can provide a straightforward and informative description of the structural behavior immediately after an earthquake. Methods based on capacity curve have been proposed in previous studies for building damage evaluation for mainshock and aftershock. However, several issues, such as the automated derivation of the capacity curve, the sensors placement with limited sensors and the comparison of the damage evaluation results with those using existing codes or guidelines, hinder its practical use in the application of SHM. This dissertation is devoted to address these issues.

First, an automated method for the derivation of the capacity curve from measured structural acceleration response is presented. Based on the decomposition by wavelet transform method, the structural behavior is directly evaluated in the form of a capacity curve of the predominant response, as a relationship between the spectral force and spectral

displacement. It enables the user to judge the performance of the building quickly after an earthquake. The feasibility of the proposed method is demonstrated through numerical simulations, full-scale shaking-table tests, and actual response of a steel tower during 2016 Fukushima earthquake.

Then, a strategy based on the piece-wise cubic polynomial interpolation (PWCPI) procedure is proposed to estimate the capacity curve for high-rise buildings from accelerations using limited sensors placed at regular intervals along the height of the building. One salient merit of this method is that detail information of the instrumented building is not needed. Numerical simulations and shaking table tests demonstrated that the proposed method could provide a satisfactory estimate of capacity curve with a few sensors.

Finally, validations for capacity-curve-based (CCB) method for post-earthquake damage evaluation framework are conducted using field survey results, full-scale shaking table tests and numerical simulations. Comparisons between the CCB method and conventional visual inspection-based method are made. It is shown that the damage evaluation results using the CCB method agree fairly well with those of visual inspection, indicating that the CCB method could serve as a useful tool for post-earthquake damage evaluation.

Acknowledgements

I would like to express my sincere gratitude to my supervisor Prof. Koichi Kusunoki for providing me a chance to carry on research on structural health monitoring in the University of Tokyo. I am grateful for his continuous support and great guidance throughout the course of my research. I would also like to thank my committee members, Prof. Fujita, Prof. Iyama, Prof. Itoi and Prof. Nagayama, for their valuable comments and suggestions.

I would like to thank Kosuke Satake, Makoto Ogawa, Jiehui Wang, Zelin Wang, Dr. Hongqi Diao and other members of Kusunoki Lab for their friendly supports and help in my life in Japan. I would also like to thank Dr. Trevor Zhiqing Yeow for kindly sharing his code and constructive comments during this investigation.

My thanks also go to my friends in Japan, Yifeng Liu, Haoyu Li, Ke Gu, Dianchao Wang, Lilin Wang, Wenbo Wang, Jiaqi Zhang, Yandong Wang and others, who made my PhD life joyful and memorable.

Hearty thanks are due to Prof. Zhuangning Xie (South China University of Technology, China), Prof. Heqing Mu (South China University of Technology, China), Prof. Fengliang Zhang (Harbin Institute of Technology, China), Prof. Ka-Veng Yuen (University of Macau, China) and Prof. Siu-Kui Au (Nanyang Technological University, Singapore). I have benefited a lot from their philosophical thinking and would like to thank them for the ongoing encouragement since my graduate studies.

Special thanks go to Binbin Chen (South China University of Technology, China) for his helping hand when I was learning OPENSEES.

My studies are supported by China Scholarship Council (CSC). This support is greatly appreciated.

Last but not the least, I am deeply grateful to my parents and X Li for their understanding, patience and endless support in the pursuit of my academic dream.

Content

Chapter 1. Introduction

1.1. Post-earthquake damage evaluation

After an earthquake happens, rapid and quantitative damage evaluation for existing buildings is an imperative step to reassure the quake-affected residents. Traditionally, post-earthquake damage evaluation is carried out by visual inspection, which is widely adopted around the world([1]-[3]). In Japan, the damage evaluation process includes a quick inspection and a more detailed damage survey[2] (Figure 1-1). The trained engineers and researchers need to go to the earthquake site and evaluate the damage condition of the building one by one. The results of the quick inspections are posted on the building to remind the residents in a form of colored post-evaluation placards, in which damage classes are divided into three classes, inspected, limited entry and unsafe(Figure 1-2). For the detailed damage survey, the damage of each structural member of the building is investigated and classified into five different damage classes ranging from I (slight damage) to V (collapse). The residual seismic capacity ratio index R is estimated according to the damage condition of the members, represented by seismic capacity reduction factor η (see Table 1-1). Based on R, the damage condition of the entire structure can be judged. The evaluation result could be used for judging the appropriateness of continued long-term use of the buildings. However, this method is costly and time-consuming, especially for high-rise buildings. For instance, it took nearly 30 days for over 320 researchers and engineers to conduct field survey of damaged area after Japan 2011 Tohoku earthquake[4]. Another issue in visual inspection is that damage assessment would largely depend on subjective judgement by engineers, which varies from person to person and thus might sometimes lead to unreliable results.

Non-destructive damage detection methods such as acoustic methods, magnetic field methods and thermal field methods are able to detect damage invisible to naked eyes[5]. For this kind of methods, a priori knowledge of possible damage location is required and the portion being inspected is also need to be accessible, which hinders its use in the post-earthquake damage evaluation.

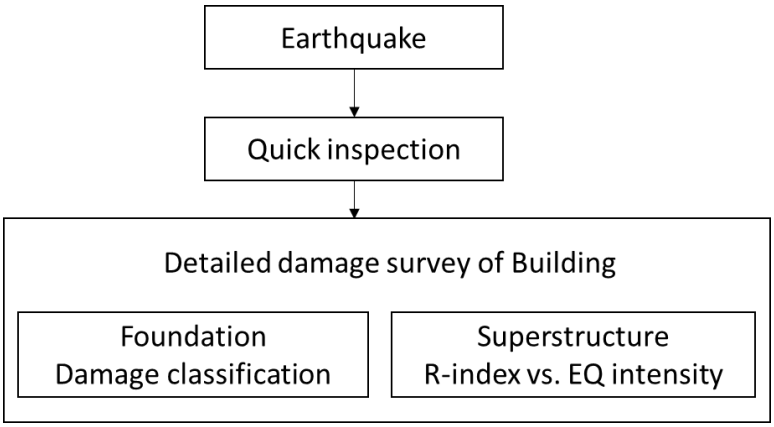

Figure 1-1 Damage evaluation process in Japan

Figure 1-2 Post-evaluation placards after quick inspection[6]

Table 1-1 Damage class definition with the seismic capacity reduction factor η for ductile reinforced concrete columns[2]

Damage class, j	Description of damage	η_j
0	No damage	1.0
I	Visible narrow cracks on the concrete surface	0.95
II	Visible clear cracks on the concrete surface	0.75
III	Local crush of cover concrete	0.5
IV	Significant crush of concrete with reinforcing bar exposure; Spalling of concrete cover	0.1
V	Buckling of the reinforcing bars; Significant damage to the core concrete; Visible vertical and/or lateral deformation of the column; Visible settlement and/or leaning of the building	0

Rapid development in sensor technologies has made it possible to use measured data from instrumented buildings and infrastructures to diagnose the condition of a structure shortly after a hazard event, which is commonly known as structural health monitoring (SHM). Under the assumption that damage to a structure can lower its natural frequencies, increase the modal damping or alter the mode shapes, methods based on the change of modal parameters ([7]-[11]) abound and play key roles in the applications of damage evaluation. For example, Beck and Jennings (1980) [7] developed a new algorithm to determine the optimal estimates of the modal parameters. They applied this method to simulated data, as well as a multi-storey building using records from the 1971 San Fernando earthquake in California. Hassiotis and Jeong (1993) [8] proposed a method for the estimation of

structural damage using measured changes in the natural frequencies. Numerical tests on a beam and a frame were used to validate the method. It is found that, by using exact or noise-polluted natural frequency data, reduction in the stiffness of up to 40% at single or multiple sites is detected. Celebi et al (2016) [11] investigated the behavioral aspects of 29-story and 30-story neighboring buildings in the Shinjuku area of Tokyo, Japan, using records retrieved from before, during, and after the main shock of the 2011 Tohoku earthquake. The results show that fundamental translational and torsional frequencies identified are much smaller for main shock and all events that followed during a period of 21 months as compared to an event two days before the main shock. However, it should be noted that the modal characteristic could be affected by the fluctuation of environmental factors, such as temperature and relative humidity ([12][13]) resulting in concerns about using changes of modal properties to quantify the damaged condition of structure. In [12], a reinforced concrete slab was built and placed outside the laboratory, and periodically vibration tested for nearly two years. The result showed that the frequencies had a strong negative correlation with temperature and humidity, damping ratios had a positive correlation, but the correlation of mode shapes with temperature and humidity change cannot be shown clearly. It is also questionable that whether the modal analysis-based methods are suitable for nonlinear cases, because strictly speaking, modal properties only exist in linear systems[14]. Meanwhile, the modal-based methods, which usually utilize Fourier transform, can only provide average temporal information, while the time-varying nature of a nonstationary signal, like the response of the structure to a strong ground motion, could be neglected. In recent years, more time-frequency techniques such as short-time Fourier transform (STFT), Hilbert-Huang transform, and wavelets have been applied to

damage detection[15]. For example, Hera and Hou (2004)[16] applied wavelet analysis on a four-story building subjected to simulated stochastic wind loading for damage detection. It was found that the damaged region can be spotted by the spatial distribution pattern of the observed spikes in the wavelet details. Khatam et al. (2007)[17] identified damage in a beam subjected to harmonic loads by detecting sudden changes in the spatial variation of transformed response. The reader can consult Kim and Melhem (2004)[18] for a more comprehensive review on damage detection by wavelet analysis.

For seismic-excited structures, it is more desired to identify the structural nonlinear behaviors, because the initiation and development of damage is a typical nonlinear process. Tomlinson and Wooden (2000) introduced numerous methods for detection, identification and modeling of nonlinear systems in [19]. Yang et al. (2007)[20] proposed a recursive least-squares estimation with unknown inputs (RLSE-UI) approach capable of identifying the structural parameters, such as the stiffness, damping and other nonlinear parameters and their variation due to damages. Bolourchi et al. (2015)[21] presented a hybrid computational method for the data-driven model free identification of nonlinear systems that characterize certain hysteretic systems. Zhou et al (2015)[22] proposed a physical parameter identification method for a nonlinear hysteretic structure with pinching behavior. The identification procedure is based on the overall least squares linear regression and hypothesis testing and the hysteresis loop is reconstructed using recorded data. The method is able to capture nonlinear behavior and structural parameters, such as pre-yielding stiffness, post-yielding stiffness and cumulative plastic deformation, directly relevant to damage and performance. Other methods focusing on parametric identification of an

assumed nonlinear model, such as the Bouc-Wen hysteretic model, have been widely reported in literature ([23]-[26]).

It is also worthy to note that the practice of artificial intelligence (AI) have received tremendous attentions in structural engineering, especially SHM in recent years[27]. Compared with conventional methods, AI methods, such as artificial neural networks (ANN)[28], support vector machine (SVM)[29], principal component analysis (PCA)[30], and low-rank matrix decomposition[31] display better performance at dealing with problems with uncertainties and insufficient information. There is also a growing interest in the use of deep learning, e.g., convolutional neural networks (CNN) in the application in SHM([32]-[36]). One salient merit of CNN is that it is more effective to learn, extract and classify the features of damaged structure. Several studies adopted CNN in structural engineering has been reported in the last few years. Sarkar et al. (2016) [32]applied CNN for characterize the damage for cracks on a composite material. The results demonstrated high characterization accuracy over different loading conditions with a few labeled training image data. Lin et al (2017) [33] developed a damage detection approach to automatically extract features from low-level sensor data through CNN. Excellent localization accuracy was shown on both noise-free and noisy data set, in contrast to another detector using wavelet packet component energy as the input feature. They also found the learned features evolve with the depth from rough filters to the concept of vibration mode, implying the good performance results from its ability to learn essential characteristics behind the data.

Lee et al (2018)[34] used a ten bar truss example to show condition for neural networks, and role of hyper-parameters when applying CNN in the structures.

1.2. Seismic effect on buildings under mainshock-aftershock sequence

Past experience around the world, e.g. in Japan (Kobe, 1995; Tohoku, 2011, Kumamoto, 2016) and China (Sichuan, 2008; Yunnan, 2013) has shown that buildings in earthquake-prone regions are often exposed to mainshock-aftershock sequences rather than a single seismic event. Therefore, after an earthquake happens, it is important to quickly assess whether the existing buildings could withstand the aftershock shaking.

A number of studies have been conducted on the influences of aftershocks on single-degree-of-freedom (SDOF) systems ([37]-[41]) as well as multi-degree-of-freedom (MDOF) systems([42]-[48]). Mahin (1980)[37] investigated analytically the response of elastoplastic SDOF systems under the mainshock-aftershock ground motions recorded at 1972 Managua earthquake. It was shown that the displacement ductility demand may slightly increase at the end of the aftershock with respect to the mainshock. Aschheim and Black (1999)[38] examined the effects of the prior earthquake damage on SDOF stiffness degrading structures and concluded that prior ductility demand has a very minor influence on peak displacement response. It was assumed that the prior displacement demands were less than those that would result if the structure was initially undamaged. An important finding includes that aftershock effects are influenced by their frequency content with respect to structural properties of a damaged building due to a mainshock[43]. Zhai et al. (2015) [41] indicated that the strong aftershock ground motion has more obvious influences on strength reduction factors in short period region than on those in long period region. Elnashai et al. (1998)[45]assessed an updated database of seismic records from Europe, California and Japan, observed that the ductility demand required by multiple earthquake ground motions can be remarkably higher than that required by a single event.

The permanent displacements triggered after the mainshock do not significantly increase as a consequence of the aftershock when the structure has degrading hysteretic features, which can be explained because of the inherent self-centering capacity in the hysteresis loops[46]. Nonlinear analysis of eight RC frames by Hatzigeorgiou and Liolios (2010) under five real and 40 artificial earthquake sequences found more cumulative damage and higher structural response in all of the buildings when they were subjected to an earthquake sequence compared with a single event[44].

Fragility assessment has received much attention for evaluation of the seismic performance of structures. A fragility function allows one to map an intensity measure (IM) (generally the spectral acceleration at the first mode period) of the ground motion or an engineering demand parameter (EDP) such as peak story drift ratio or absolute floor acceleration of the structure to a damage state (DS) in order to predict the probability of the structure being in a specific damage state, such as slight, moderate, or severe damage[52]. This method has not only been applied to damage due to main shock, but also aftershock([47]-[51]). Li et al (2014)[48] investigated the collapse probability of mainshock-damaged steel buildings in aftershocks, which is a part of a framework to integrate aftershock seismic hazard into performance-based engineering (PBE). It is found that structural collapse capacity may be lower sharply when the building is exposed to a high intensity mainshock. Therefore, it may be possible that the structure collapses even if only a small aftershock follows the mainshock. Raghunandan (2015) [51] quantified the aftershock vulnerability of four modern ductile reinforced concrete framed buildings in California by performing incremental dynamic analysis of nonlinear MDOF analytical models. Collapse and damage fragility curves are generated for intact and damaged buildings, based on the nonlinear

dynamic analysis results. The results indicated that damage indicators related to the drift experienced by the damaged building best predicted the reduced aftershock collapse capacities for these ductile structures. Wen et al (2017) [49]proposed framework for the vulnerability assessment of structure under the mainshock-aftershock sequences. They applied it on a case-study reinforced concrete (RC) frame structure with 5 stories and studied the influences of aftershocks on the fragility of structure for different limit states. The effects of aftershocks on the fragility of structure are more obvious for the case that mainshock fragility changes from 30% to 60%, and the maximum influence of aftershock can exceed 15%. However, the fragility assessment requires prior knowledge on building structures and a numerical model of the building is needed. Thus it is computationally expensive. In addition, this process does not make use of response from the instrumented structure and may not reflect the real structural condition under seismic excitations.

1.3. Capacity-curve-based (CCB) damage evaluation

The capacity spectrum method (CSM) proposed by Freeman in the 1970s ([53][54]), has been served as an important tool for seismic assessment in earthquake engineering nowadays and adopted as the basis of building codes and guidelines in many countries worldwide ([55]-[57]). This method is to compare the capacity of buildings in a form of a pushover curve with demands on the structure in the form of a design spectrum or the response spectrum of an actual ground motion. The graphical intersection of the two curves approximates the structural response under excitations. Specifically, it consists of the following step[58]:

1. Develop the relationship between base shear and roof displacement, called as the pushover curve.
2. Convert the pushover curve to a capacity diagram.
3. Convert the elastic response or design spectrum for the standard pseudo acceleration, *A*, versus natural period, T_n, format to the *A*-*D* format, where *D* is the deformation spectrum ordinate, to obtain the demand diagram.
4. Plot the demand diagram and capacity diagram together and determine the displacement demand. In this step, dynamic analyses are needed with successively updated values of the natural frequency and equivalent viscous damping. The earthquake-induced deformation of an inelastic SDOF system can be estimated by an iterative method which requires the analysis of a sequence of equivalent linear SDOF systems with added equivalent viscous damping to account for post-yield energy dissipation.
5. Convert the displacement demand obtained in step 4 to global (roof) displacement and individual component deformation and compare them to the limiting values for the specified performance goals.

For the application of estimating capacity curve using recorded response from structures, the early work can be found in ([59][60]) for the monitoring of Millikan Library building, Bank of California Building and Imperial County Services building and some recent practice can be found in ([61]-[66]).

Recently, Kusunoki (2018)[61][62] proposed a framework for post-earthquake damage evaluation based on capacity curve which utilize the measured data from instrumented buildings. This method can evaluate the damage for mainshock and aftershock by using

seismic response data from mainshock. Figure 1-3 illustrates the concept of the method based on the capacity curve method. The capacity curve here is obtained from the recorded accelerations of the instrumented building, in which the displacements are obtained by the double integral using a wavelet transform. The demand curve is also derived from the ground acceleration and the curve with 5% viscous damping is usually adopted for elastic range. When the structural behavior is nonlinear, an additional damping effect is considered. Then, the demand curve is reduced from the 5% elastic demand curve, as shown in Figure 1-3. The intersection of the capacity curve and the reduced demand curve is the predicted maximum response during the mainshock. In practice, the maximum deformation of capacity curve estimated from measured seismic can be considered as the maximum response under the mainshock and thus demand curve is not needed. Similarly, this method can also be extended to predict the maximum response during a MA sequence by considering the mainshock and its subsequent aftershock as a single earthquake input. Given that the input energy of the combined earthquake is greater than that of the mainshock alone, the maximum response of the former would usually be greater. One simple method of accounting for this in the capacity spectrum is to reduce the equivalent damping and the subsequent reduction in demand, as indicated in Figure 1-3. The predicted maximum response during the MA sequence is the intersection of the demand curve and the capacity curve and then the damage class can be judged.

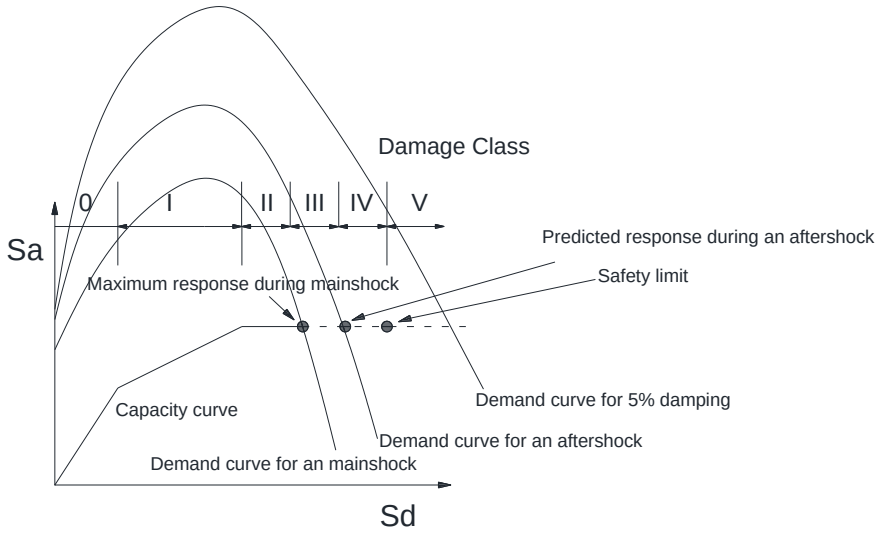

Figure 1-3 Concept of the CCB method[61][62]

However, in order to make this method more practical in the post-earthquake damage evaluation, there are some issues that need to be solve:

1. To generate capacity curve, selection of cutting off frequencies is crucial for filtering the noise of the measured response in the displacement reconstruction and isolating the first mode response of the structure. Inappropriate cutoff frequency may lead to undesirable errors, such as reduction in the estimation of the maximum response and altering of the hysteretic path of the hysteretic response[63]. In previous studies, filters[60] or wavelet transform [64][65]is often adopted to extract the first mode component. However, the frequency band selection process before was based on visual judgement from Fourier amplitude spectrum of the response or manual trial and error tests, which creates difficulty in the practical monitoring of different structures.

2. For estimating the capacity curve, floor accelerations from instrumented building are required. Therefore, in previous studies, each floor of the building had instrumented sensors. However, in real applications, issues may arise during sensor installation, especially for high-rise buildings, where the number of sensors is limited owing to budget and accessibility. Typically, the responses of noninstrumented floors could be obtained using the piece-wise cubic polynomial interpolation (PWCPI) procedure ([67][68]) or mode-based interpolation procedure ([69][70]). Although these response reconstruction approaches work well in the linear-elastic range, their accuracies in the nonlinear range have not been validated. Another issue related to interpolation is the selection of appropriate locations for sensor installation. In the past two decades, research on optimal sensor placement (OSP) on structures have gained considerable attention ([71]-[74]). However, most OSP methods require model properties, such as stiffness and mass distribution of structures, which are difficult to obtain in most cases.
3. Damage assessment results are usually compared with experiments or numerical results in previous studies [75][76]. In the case of real world diagnosis, it is always desirable to compare the damage identification results with the code-specified damage classifications, but to the author's knowledge, few publications have addressed this issue. The availability of the capacity-curve-based (CCB) method still needs to be tested.

Regarding the above mentioned research background, the research in this paper is carried out.

1.4. Objectives

The main goal of this dissertation is to develop a rapid and reliable methodology for estimating capacity curve using wavelet transform for damage evaluation with limited number of accelerometers and validate the CCB method. The objective of this study is realized through the completion of the following task:

1. Develop an automatic algorithm to estimate capacity curve using recorded seismic accelerations.
2. Develop a strategy to estimate the capacity curve for high-rise buildings with limited number of accelerometers.
3. Validate the CCB method using field survey results, shaking table tests and numerical simulations.

1.5. Organization

This dissertation is organized as follows:

Chapter 2 presents an automated method for derivation of capacity curve from measured structural acceleration response. Based on the decomposition by wavelet transform method, the structural behavior is directly evaluated in the form of a capacity curve of the predominant response, as a relationship between the spectral force and spectral displacement. It enables the user to judge the performance of the building quickly after an earthquake. The feasibility of the proposed method is demonstrated through numerical simulations, full-scale shaking-table tests, and actual response of a steel tower during 2016 Fukushima earthquake.

Chapter 3 proposes a strategy based on the piece-wise cubic polynomial interpolation (PWCPI) procedure to estimate the capacity curve for high-rise buildings from accelerations using limited sensors placed at regular intervals along the height of the building. The validity of the method is assessed by numerical simulations and shaking table tests.

Chapter 4 presents validations for CCB method via field survey results, full-scale shaking table tests and a numerical simulation study for damage evaluation for mainshock and aftershock damage prediction. Comparisons between the CCB method and conventional visual inspection-based method are made.

Chapter 5 gives a summary of the conclusions and provides suggestions for future work.

1.6. References

[1] Rojahn C. "Procedures for post-earthquake safety evaluation of buildings, ATC-20. Technical Report." *Applied Technology Council (ATC), Redwood City, CA*, 1989.

[2] Nakano, Yoshiaki, et al. "Guideline for post-earthquake damage evaluation and rehabilitation of RC buildings in Japan." *13th World Conference on Earthquake Engineering*. No. 124. 2004.

[3] Baggio, Carlo, et al. "Field Manual for post-earthquake damage and safety assessment and short term countermeasures (AeDES)." *European Commission—Joint Research Centre—Institute for the Protection and Security of the Citizen, EUR* 22868 (2007).

[4] Architectural Institute of Japan (AIJ). "Preliminary Reconnaissance Report of the 2011 Tohoku-Chiho Taiheiyo-Oki Earthquake. " Springer, 2012.

[5] Rens, Kevin L., Terry J. Wipf, and F. Wayne Klaiber. "Review of nondestructive evaluation techniques of civil infrastructure." *Journal of performance of constructed facilities* 11, no. 4 (1997): 152-160.

[6] Hiroki Sunohara. “Post-earthquake building damage assessment and new technologies in Japan.” *Global Connections Day, ICC Annual Conference at Richmond, VA*, (2018) https://cdn-web.iccsafe.org/wp-content/uploads/Hiroki-Sunohara.pdf

[7] Beck, James L., and Paul C. Jennings. "Structural identification using linear models and earthquake records." *Earthquake engineering & structural dynamics* 8.2 (1980): 145-160.

[8] Hassiotis, S., and G. D. Jeong. "Assessment of structural damage from natural frequency measurements." *Computers & structures*49.4 (1993): 679-691.

[9] Kohler, Monica D., Paul M. Davis, and Erdal Safak. "Earthquake and ambient vibration monitoring of the steel-frame UCLA Factor building." *Earthquake Spectra* 21.3 (2005): 715-736.

[10] Farrar, Charles R., and Keith Worden. *Structural health monitoring: a machine learning perspective*. John Wiley & Sons, 2012.

[11] Çelebi, Mehmet, et al. "Responses of two tall buildings in Tokyo, Japan, before, during, and after the M9. 0 Tohoku Earthquake of 11 March 2011." *Earthquake Spectra* 32.1 (2016): 463-495.

[12] Xia, Yong, et al. "Long term vibration monitoring of an RC slab: temperature and humidity effect." *Engineering Structures* 28.3 (2006): 441-452.

[13] Kim, Jeong-Tae, Jae-Hyung Park, and Byung-Jun Lee. "Vibration-based damage monitoring in model plate-girder bridges under uncertain temperature conditions." *Engineering Structures* 29.7 (2007): 1354-1365.

[14] Hernandez, Eric M., and Geoff May. "Dissipated energy ratio as a feature for earthquake-induced damage detection of instrumented structures." *Journal of Engineering Mechanics*139.11 (2012): 1521-1529.

[15] Nagarajaiah, Satish, and Biswajit Basu. "Output only modal identification and structural damage detection using time frequency & wavelet techniques." *Earthquake Engineering and Engineering Vibration* 8, no. 4 (2009): 583-605.

[16] Hera, Adriana, and Zhikun Hou. "Application of wavelet approach for ASCE structural health monitoring benchmark studies." *Journal of Engineering Mechanics* 130, no. 1 (2004): 96-104.

[17] Khatam, Hamed, Ali Akbar Golafshani, S. B. Beheshti-Aval, and Mohammad Noori. "Harmonic class loading for damage identification in beams using wavelet analysis." *Structural Health Monitoring* 6, no. 1 (2007): 67-80.

[18] Kim, Hansang, and Hani Melhem. "Damage detection of structures by wavelet analysis." *Engineering Structures* 26, no. 3 (2004): 347-362.

[19] Tomlinson, G. R., and K. Worden. *Nonlinearity in structural dynamics: detection, identification and modelling*. CRC Press, 2000.

[20] Yang, Jann N., Shuwen Pan, and Silian Lin. "Least-squares estimation with unknown excitations for damage identification of structures." *Journal of Engineering Mechanics* 133, no. 1 (2007): 12-21.

[21] Bolourchi, Ali, Sami F. Masri, and Osama J. Aldraihem. "Studies into computational intelligence and evolutionary approaches for model-free identification of hysteretic systems." *Computer-Aided Civil and Infrastructure Engineering* 30, no. 5 (2015): 330-346.

[22] Zhou, Cong, et al. "Physical parameter identification of structural systems with hysteretic pinching." *Computer‐Aided Civil and Infrastructure Engineering* 30.4 (2015): 247-262.

[23] Chatzi, Eleni N., Andrew W. Smyth, and Sami F. Masri. "Experimental application of on-line parametric identification for nonlinear hysteretic systems with model uncertainty." *Structural Safety* 32, no. 5 (2010): 326-337.

[24] Charalampakis, A. E., and C. K. Dimou. "Identification of Bouc–Wen hysteretic systems using particle swarm optimization." *Computers & structures* 88, no. 21-22 (2010): 1197-1205.

[25] Chatzis, Manolis N., and Eleni N. Chatzi. "A discontinuous unscented Kalman filter for non-smooth dynamic problems." *Frontiers in Built Environment* 3 (2017): 56.

[26] Wang, Li, and Zhong-Rong Lu. "Identification of Bouc-Wen hysteretic parameters based on enhanced response sensitivity approach." In *Journal of Physics: Conference Series*, vol. 842, no. 1, p. 012021. IOP Publishing, 2017.

[27] Salehi, Hadi, and Rigoberto Burgueno. "Emerging artificial intelligence methods in structural engineering." *Engineering structures* 171 (2018): 170-189.

[28] Yan, Bo, et al. "Beam structure damage identification based on BP neural network and support vector machine." *Mathematical Problems in Engineering* 2014 (2014).

[29] Gui, Guoqing, et al. "Data-driven support vector machine with optimization techniques for structural health monitoring and damage detection." *KSCE Journal of Civil Engineering* 21.2 (2017): 523-534.

[30] Tibaduiza, Diego A., et al. "Structural damage detection using principal component analysis and damage indices." *Journal of Intelligent Material Systems and Structures* 27.2 (2016): 233-248.

[31] Nagarajaiah, Satish, and Yongchao Yang. "Modeling and harnessing sparse and low‐rank data structure: a new paradigm for structural dynamics, identification, damage detection, and health monitoring." *Structural Control and Health Monitoring* 24.1 (2017): e1851.

[32] Sarkar, Soumalya, et al. "Deep learning for structural health monitoring: A damage characterization application." *Annual Conference of the Prognostics and Health Management Society*. 2016.

[33] Lin, Yi‐zhou, Zhen‐hua Nie, and Hong‐wei Ma. "Structural damage detection with automatic feature‐extraction through deep learning." *Computer‐Aided Civil and Infrastructure Engineering* 32.12 (2017): 1025-1046.

[34] Lee, Seunghye, et al. "Background information of deep learning for structural engineering." *Archives of Computational Methods in Engineering* 25.1 (2018): 121-129.

[35] Abdeljaber, Osama, et al. "Real-time vibration-based structural damage detection using one-dimensional convolutional neural networks." *Journal of Sound and Vibration* 388 (2017): 154-170.

[36] Avci, Onur, et al. "Structural damage detection in real time: implementation of 1D convolutional neural networks for SHM applications." *Structural Health Monitoring & Damage Detection, Volume 7. Springer, Cham*, 2017. 49-54.

[37] Mahin, Stephen A. "Effects of duration and aftershocks on inelastic design earthquakes." *Proceedings of the 7th world conference on earthquake engineering*. Vol. 5. 1980.

[38] Aschheim, Mark, and Edgar Black. "Effects of prior earthquake damage on response of simple stiffness-degrading structures." *Earthquake Spectra* 15.1 (1999): 1-24.

[39] Goda, Katsuichiro. "Nonlinear response potential of mainshock–aftershock sequences from Japanese earthquakes." *Bulletin of the Seismological Society of America*102.5 (2012): 2139-2156.

[40] Goda, Katsuichiro, and Colin A. Taylor. "Effects of aftershocks on peak ductility demand due to strong ground motion records from shallow crustal earthquakes." *Earthquake Engineering & Structural Dynamics* 41.15 (2012): 2311-2330.

[41] Zhai, Chang-Hai, et al. "The ductility-based strength reduction factor for the mainshock–aftershock sequence-type ground motions." *Bulletin of Earthquake Engineering* 13.10 (2015): 2893-2914.

[42] Ruiz-García, Jorge, and Juan C. Negrete-Manriquez. "Evaluation of drift demands in existing steel frames under as-recorded far-field and near-fault mainshock–aftershock seismic sequences." *Engineering Structures* 33.2 (2011): 621-634.

[43] Li, Quanwang, and Bruce R. Ellingwood. "Performance evaluation and damage assessment of steel frame buildings under main shock–aftershock earthquake sequences." *Earthquake engineering & structural dynamics* 36.3 (2007): 405-427.

[44] Hatzigeorgiou, George D., and Asterios A. Liolios. "Nonlinear behaviour of RC frames under repeated strong ground motions." *Soil Dynamics and Earthquake Engineering* 30.10 (2010): 1010-1025.

[45] Elnashai, A. S., J. J. Bommer, and A. Martinez-Pereira. "Engineering implications of strong-motion records from recent earthquakes." *Proceedings of 11th European conference on earthquake engineering*. 1998.

[46] Ruiz-García, J. "Issues on the response of existing buildings under mainshock–aftershock seismic sequences." *15th World conference on earthquake engineering*. 2012.

[47] Shin, Jiuk, JunHee Kim, and Kihak Lee. "Seismic assessment of damaged piloti-type RC building subjected to successive earthquakes." *Earthquake engineering & Structural dynamics*43.11 (2014): 1603-1619.

[48] Li, Yue, Ruiqiang Song, and John W. Van De Lindt. "Collapse fragility of steel structures subjected to earthquake mainshock-aftershock sequences." *Journal of Structural Engineering*140.12 (2014): 04014095.

[49] Wen, Weiping, et al. "Framework for the vulnerability assessment of structure under mainshock-aftershock sequences." *Soil Dynamics and Earthquake Engineering* 101 (2017): 41-52.

[50] Jalayer, Fatemeh, and Hossein Ebrahimian. "Seismic risk assessment considering cumulative damage due to aftershocks." *Earthquake Engineering & Structural Dynamics*46.3 (2017): 369-389.

[51] Raghunandan, Meera, Abbie B. Liel, and Nicolas Luco. "Aftershock collapse vulnerability assessment of reinforced concrete frame structures." *Earthquake Engineering & Structural Dynamics* 44.3 (2015): 419-439.

[52] Noh, Hae Young, et al. "Development of fragility functions as a damage classification/prediction method for steel moment-resisting frames using a wavelet-based damage sensitive feature." *Earthquake Engineering & Structural Dynamics* 41.4 (2012): 681-696.

[53] Freeman, S.A., Nicoletti, J.P. and Tyrell, J.V. "Evaluation of Existing Buildings for Seismic Risk—A Case Study of Puget Sound Naval Shipyard." *Bremerton, Washington. Proceedings of U.S. National Conference on Earthquake Engineering, Berkeley,* (1975) 113-122.

[54] Freeman, Sigmund A. "Prediction of response of concrete buildings to severe earthquake motion." *Special Publication* 55 (1978): 589-606.

[55] ATC-40. Seismic Evaluation and Retrofit of Concrete Building. Applied Technology Council, Redwood City,California, 1996.

[56] Midorikawa, Mistumasa, et al. "Performance-based seismic design code for buildings in Japan." *Earthquake Engineering and Engineering Seismology* 4.1 (2003): 15-25.

[57] Wilson, John L., Nelson TK Lam, and Lam Pham. "Development of the new Australian earthquake loading standard." *EJSE Special Issue: Earthquake Engineering*

in the low and moderate seismic regions of Southeast Asia and Australia 8 (2008): 25-31.

[58] Chopra, Anil K., and Rakesh K. Goel. "Capacity-demand-diagram methods based on inelastic design spectrum." *Earthquake spectra* 15.4 (1999): 637-656.

[59] Iemura, H., and P. C. Jennings. "Hysteretic response of a nine-storey reinforced concrete building." *Earthquake Engineering & Structural Dynamics* 3, no. 2 (1974): 183-201.

[60] Iwan, Wilfred D., and Arturo O. Cifuentes. "A model for system identification of degrading structures." *Earthquake engineering & structural dynamics* 14, no. 6 (1986): 877-890.

[61] Kusunoki, “Development of Building Monitoring System to Evaluate Residual Seismic Capacity after an Earthquake.” *News Letter Plus, Earthquake Research Institute, The University of Tokyo,* no.29 (2018)

[62] Kusunoki, Koichi, et al. "A new method for evaluating the real-time residual seismic capacity of existing structures using accelerometers: Structures with multiple degrees of freedom." *Japan Architectural Review* 1.1 (2018): 77-86.

[63] Dowgala, Jeffrey David. *Detecting and quantifying damage in buildings using earthquake response data and capacity curves*. Diss. Purdue University, 2013.

[64] Kusunoki, Koichi, et al. "Evaluation of structural condition using Wavelet transforms." *14th World Conference on Earthquake Engineering, Beijing, China*. 2008.

[65] Kusunoki, Koichi, Akira Tasai, and Masaomi Teshigawara. "Development of building monitoring system to evaluate residual seismic capacity after an

earthquake." *Proceedings of the fifteenth world conference on earthquake engineering, Lisbon, Portugal*. 2012.

[66] Kusunoki, Koichi, “Damage evaluation of a base-isolated building with measured accelerations during tohoku earthquake.” *Proceedings of the sixteenth world conference on earthquake engineering, Santiago, Chile*. 2017.

[67] Limongelli, Maria Pina. "Optimal location of sensors for reconstruction of seismic responses through spline function interpolation." *Earthquake engineering & structural dynamics*32.7 (2003): 1055-1074.

[68] Meo, Michele, and G. Zumpano. "On the optimal sensor placement techniques for a bridge structure." *Engineering structures* 27.10 (2005): 1488-1497.

[69] Goel, Rakesh K. "Mode-based procedure to interpolate strong motion records of instrumented buildings." *ISET Journal of Earthquake Technology* 45.3-4 (2008): 97-113.

[70] Mita, Akira, Kenta Hirai, and Sayuki Ozawa. "Design strategy of structural health monitoring system consisting of four sensors for tall buildings." *8th European Workshop on Structural Health Monitoring, EWSHM 2016*. NDT. net, 2016.

[71] Papadimitriou, Costas. "Optimal sensor placement methodology for parametric identification of structural systems." *Journal of sound and vibration* 278.4-5 (2004): 923-947.

[72] Yi, Ting-Hua, Hong-Nan Li, and Ming Gu. "Optimal sensor placement for structural health monitoring based on multiple optimization strategies." *The Structural Design of Tall and Special Buildings* 20.7 (2011): 881-900.

[73] Yi, Ting-Hua, Hong-Nan Li, and Xu-Dong Zhang. "Sensor placement on Canton Tower for health monitoring using asynchronous-climb monkey algorithm." *Smart Materials and Structures* 21.12 (2012): 125023.

[74] Sun, Hao, and Oral Büyüköztürk. "Optimal sensor placement in structural health monitoring using discrete optimization." *Smart Materials and Structures* 24.12 (2015): 125034.

[75] Isidori, D., et al. "Proof of concept of the structural health monitoring of framed structures by a novel combined experimental and theoretical approach." *Structural control and health monitoring* 23.5 (2016): 802-824.

[76] Pierdicca, A., et al. "Damage detection in a precast structure subjected to an earthquake: A numerical approach." *Engineering Structures* 127 (2016): 447-458.

Chapter 2. A wavelet transform-based approach to estimate capacity curve

This chapter is reproduced from the paper titled "A wavelet transform based capacity curve estimation approach using seismic response data" coauthored with Koichi Kusunoki, which has been published in *Structural Control and Health Monitoring*, 25 (12), e2267, DOI: 10.1002/stc.2267

2.1. Overview

In this chapter, by making use of the superior ability of wavelet transform method (WTM) in signal reconstruction, an automated computation procedure for capacity curve from structural acceleration response is proposed. The theory of capacity estimation from measured response is first presented, followed by the algorithm for capacity curve calculation using WTM. Examples of numerical simulation, shaking table tests and field applications are presented to illustrate the approach.

2.2. Capacity curve from measured response

The capacity curve commonly obtained by pushover analysis is the relationship between base shear force, V_b, and the roof (*N*th floor) displacement, x_N of the structure. To directly compare with the demand response spectra, V_b and x_N are converted to a spectral set of coordinates S_a and S_d by using the dynamic characteristics of the fundamental mode to represent the structure as a single-degree-of freedom structure. The mass normalized S_a and S_d are given by:

$$S_{\mathrm{a}} = \frac{V_{\mathrm{b}}}{{}_1\bar{M}} \tag{2-1}$$

$$S_{\mathrm{d}} = \frac{x_{\mathrm{N}}}{\beta_1 \cdot {}_1u_{\mathrm{N}}} \tag{2-2}$$

Where ${}_1u_{\mathrm{N}}$ is the *N*th floor element of the fundamental mode $\{{}_1u\}$, β_1 is the first mode participation factor $= \frac{\sum_{i=1}^{N} m_i \cdot {}_1u_i}{\sum_{i=1}^{N} m_i \cdot {}_1u_i^2}$ (m_i=lumped mass on the *i*-th floor), and ${}_1\bar{M}$ is the equivalent mass for the first mode $= \frac{(\sum_{i=1}^{N} m_i \cdot {}_1u_i)^2}{\sum_{i=1}^{N} m_i \cdot {}_1u_i^2}$, which can be obtained using assumed mass ratios and mode shape. The mode shape can be obtained from finite element model or assumed as linear for simplicity. It can be also obtained from the fundamental-mode floor accelerations in practise.

In the case where ground motion $\ddot{x}_0$ and structural acceleration response $\ddot{x}_i$ for each floor are available, the base shear force $\tilde{V}_{\mathrm{b}}$ can be obtained by summing inertial force of each floor

$$\tilde{V}_{\mathrm{b}} = \sum_{i=1}^{N} m_i(\ddot{x}_i + \ddot{x}_0) \tag{2-3}$$

Thus, the corresponding spectral acceleration

$$\tilde{S}_{\mathrm{a}} = \frac{\sum_{i=1}^{N} m_i(\ddot{x}_i + \ddot{x}_0)}{{}_1\bar{M}} \tag{2-4}$$

In practice, it is more desired to study the fundamental mode of the response because drawing meaningful conclusions from Eq. (2-2) and Eq. (2-4) is difficult due to a number of different modes involved. By isolating the fundamental mode component, one can obtain

$$ {}_1\tilde{S}_{\mathrm{a}} = \frac{\sum_{i=1}^{N} m_i \, {}_1\{(\ddot{x}_i + \ddot{x}_0)\}}{{}_1\bar{M}} \tag{2-5} $$

$$ {}_1\tilde{S}_{\mathrm{d}} = \frac{{}_1\{x_{\mathrm{N}}\}}{\beta_1 \cdot {}_1 u_{\mathrm{N}}} \tag{2-6} $$

Where ${}_1\{\}$ denotes extracting the first mode component from the response.

Finally, the capacity curve can be found by deriving the backbone curve, i.e., points that update the maximum deformation during vibration, from ${}_1\tilde{S}_{\mathrm{a}}$, ${}_1\tilde{S}_{\mathrm{d}}$ hysteresis loops.

In principle, with measured acceleration, it is possible to get the relative displacement through numerical integration. In addition, from Eq. (2-5) and Eq. (2-6), it can be shown that m_i is not necessarily the absolute value but the relative to the total mass, which can be represented by the floor area governed by each accelerometer. Therefore, only by utilizing the acceleration response from accelerometers as well as assumed mass distribution and mode shape, the capacity curve can be calculated.

2.3. Capacity curve decomposition with the WTM

It was shown in section 2.2 that spectral displacement and acceleration can be obtained using the measured response data. The next issue is how to effectively decompose the signal and draw out useful information from measured signal. In this section, background of wavelet transform and capacity curve estimation through wavelet transform method will be described.

2.3.1 Outline of Wavelet Transform Method[1]

A wavelet is a local wave-like function with an amplitude that begins at zero, increases, and then decreases back to zero. Just as the Fourier transform decomposes the signal into

sines and cosines, WTM serves to decompose the signal into a series of basic functions of dilated and translated versions of the parent wavelet function. A main advantage of wavelet approach is that it allows for reconstructing signal perfectly, while signal leakage or phase distortion may arise when using conventional filters for signal reconstruction. The continuous wavelet transform (CWT) of a signal $f(t)$ is defined as

$$T(a,b)=\frac{1}{\sqrt{a}}\int_{-\infty}^{\infty} f(t)\psi^{*}(\frac{t-b}{a})\mathrm{d}t \tag{2-7}$$

Where a and b are dilation and translation parameters, respectively. Both are real numbers and a must be positive. $\psi^{*}(\frac{t-b}{a})$ denotes the conjugate of the dilated and translated version of selected mother wavelet $\psi(t)$. b specifies the location of the moving wavelet window in the wavelet transform, and a indicates width of the wavelet window. $T(a,b)$ reflects how well the wavelet function correlates the signal analyzed.

In practice, the dyadic grid arrangement is often employed in wavelet transform. The dilation is defined as $a=2^{j}$ and the translation parameter takes the form $b=k2^{j}$,where $(j,k)\in Z$, and Z is a set of integers. Using the discrete scales, the wavelet expansion of $f(t)$ and the coefficients of the wavelet expansion are defined as

$$f(t)=\sum_{j}\sum_{k}T_{j,k}\psi_{j,k}(t) \tag{2-8}$$

$$T_{j,k}=\int_{-\infty}^{+\infty} f(t)\psi_{j,k}^{*}(t)\mathrm{d}t \tag{2-9}$$

Where $\psi_{j,k}(t)=2^{-j/2}\psi(2^{-j/2}-k)$

In discrete wavelet transform (DWT), a signal can be represented by its approximations and details. The detail at rank j is defined as

$$D_{j}=\sum_{k\in Z}T_{j,k}\psi_{j,k}(t) \tag{2-10}$$

And the approximation at rank J is defined as

$$A_J = \sum_{j>J} D_j \tag{2-11}$$

Apparently,

$$A_{J-1} = A_J + D_J \tag{2-12}$$

And

$$f(t) = A_J + \sum_{j \le J} D_j \tag{2-13}$$

Concretely, for a signal $f_0(t)$ of N data points, the maximum decomposition rank $n = \log_2 N$ and the signal can be decomposed into different series of signals with specific Nyquist frequency.

$$f_0(t) = A_n + \sum_{j=1}^{n} D_j \tag{2-14}$$

The frequency content observed in the approximation A_n and detail D_j can be calculated as a function of the sampling rate f_s , as

$$f_{s,A} = [0, 2^{-n-1} f_s] \tag{2-15}$$

$$f_{s,D_j} = [2^{-j-1} f_s, 2^{-j} f_s] \tag{2-16}$$

2.3.2 Capacity curve calculation from measured acceleration

With WTM, Eq. (2-5) and Eq. (2-6) can be rewritten as

$${}_1\tilde{S}_{\mathrm{a}} = \frac{\sum_{i=1}^{N} m_i \sum_j (\ddot{x}^{\mathrm{W}}_{i,j} + \ddot{x}^{\mathrm{W}}_{0,j})}{{}_1\bar{M}} \tag{2-17}$$

$${}_1\tilde{S}_{\mathrm{d}} = \frac{\sum_j x^{\mathrm{W}}{}_{\mathrm{N},j}}{\beta_1 \cdot {}_1u_{\mathrm{N}}} \tag{2-18}$$

Where $\ddot{x}_{0,j}^{\mathrm{W}}$ and $\ddot{x}_{i,j}^{\mathrm{W}}$ are the *j*th rank component of measured ground motion and acceleration at *i*-th floor obtained through WTM. Due to fixed frequency resolution, the fundamental component does not always fall into one specific rank, which requires to sum up several ranks. The term $\sum_j (\ddot{x}_{i,j}^{\mathrm{W}} + \ddot{x}_{0,j}^{\mathrm{W}})$ and $\sum_j x^{\mathrm{W}}{}_{\mathrm{N},j}$ are the sum of response at several ranks to approximate the first mode component of $(\ddot{x}_i + \ddot{x}_0)$ and x_{N}, respectively.

The *j*th rank components of ${}_1\tilde{S}_{\mathrm{a}}$ and ${}_1\tilde{S}_{\mathrm{d}}$ are

$$\tilde{S}_{\mathrm{a},j} = \frac{\sum_{i=1}^{N} m_i (\ddot{x}_{i,j}^{\mathrm{W}} + \ddot{x}_{0,j}^{\mathrm{W}})}{{}_1\bar{M}} \tag{2-19}$$

$$\tilde{S}_{\mathrm{d},j} = \frac{x^{\mathrm{W}}{}_{\mathrm{N},j}}{\beta_1 \cdot {}_1u_{\mathrm{N}}} \tag{2-20}$$

The measured input acceleration at the basement $\ddot{x}_0^{\mathrm{M}}$ and the measured absolute acceleration at each floor $\ddot{X}_i^{\mathrm{M}}$, can be decomposed into each rank by WTM, as Eq. (2-21) and Eq. (2-22)

$$\ddot{x}_0^{\mathrm{M}} = \sum_{j=1}^{N} D_{\ddot{x}_0^{\mathrm{M}},j} + A_{\ddot{x}_0^{\mathrm{M}},N} \tag{2-21}$$

$$\ddot{X}_i^{\mathrm{M}} = \sum_{j=1}^{N} D_{\ddot{x}_i^{\mathrm{M}},j} + A_{\ddot{x}_i^{\mathrm{M}},N} \tag{2-22}$$

Note that the low-frequency noise component in approximations $A_{\ddot{x}_0^{\mathrm{M}},N}$ and $A_{\ddot{x}_i^{\mathrm{M}},N}$ can lead to significant errors when applying an integration procedure and thus would be neglected. Only the detail parts are used to extract the first mode component of the measured acceleration from the original signal.

$$\ddot{x}_{0,j}^{\mathrm{W}} = D_{\ddot{x}_0^{\mathrm{M}},j} \tag{2-23}$$

$$\ddot{X}_{i,j}^{\mathrm{W}} = D_{\ddot{x}_i^{\mathrm{M}},j} \tag{2-24}$$

The *j* th rank component of relative acceleration and displacement at *i*-th floor to the ground are given by follows

$$\ddot{x}_{i,j}^{\mathrm{W}} = \ddot{X}_{i,j}^{\mathrm{W}} - \ddot{x}_{0,j}^{\mathrm{W}} \tag{2-25}$$

$$x_{i,j}^{\mathrm{W}} = \iint \ddot{x}_{i,j}^{\mathrm{W}} \mathrm{d}t^2 \tag{2-26}$$

When deriving displacement from acceleration, some signal processing technique, such as demean and detrend, may be required to perform the baseline correction[2]. Substituting Eq. (2-23) ~ Eq. (2-26) to Eq. (2-19) and Eq. (2-20), the *j* th rank component of hysteretic loops can be obtained. To the choose the appropriate ranks that constitute the predominant mode, the rank with largest cyclic area representing the largest dissipated energy during vibration would be selected as the temporary predominant mode. In this step, the structural behavior would be judged as linear or nonlinear according to deviation of the largest cyclic curve. Then, if the representative linear slope of adjacent rank is similar to that of the temporary predominant rank, it would be added. Different threshold values would be chosen according to the behavior judged in the previous step. Note that once the threshold values for area ratios and slope proximity are set, the selection process can be completed automatically, without manual interference. The mother wavelet adopted in this study is B-spline wavelet of order 4. The framework of the proposed capacity estimation algorithm is shown in Figure 2-1.

Limitation may arise for close modes near the fundamental mode component, where the fundamental mode cannot be well isolated. However, given that the higher mode frequencies are normally 3 times greater than the fundamental one for most buildings[3], the first mode frequency component would fall into different ranks from higher modes, which can be extracted using the proposed method.

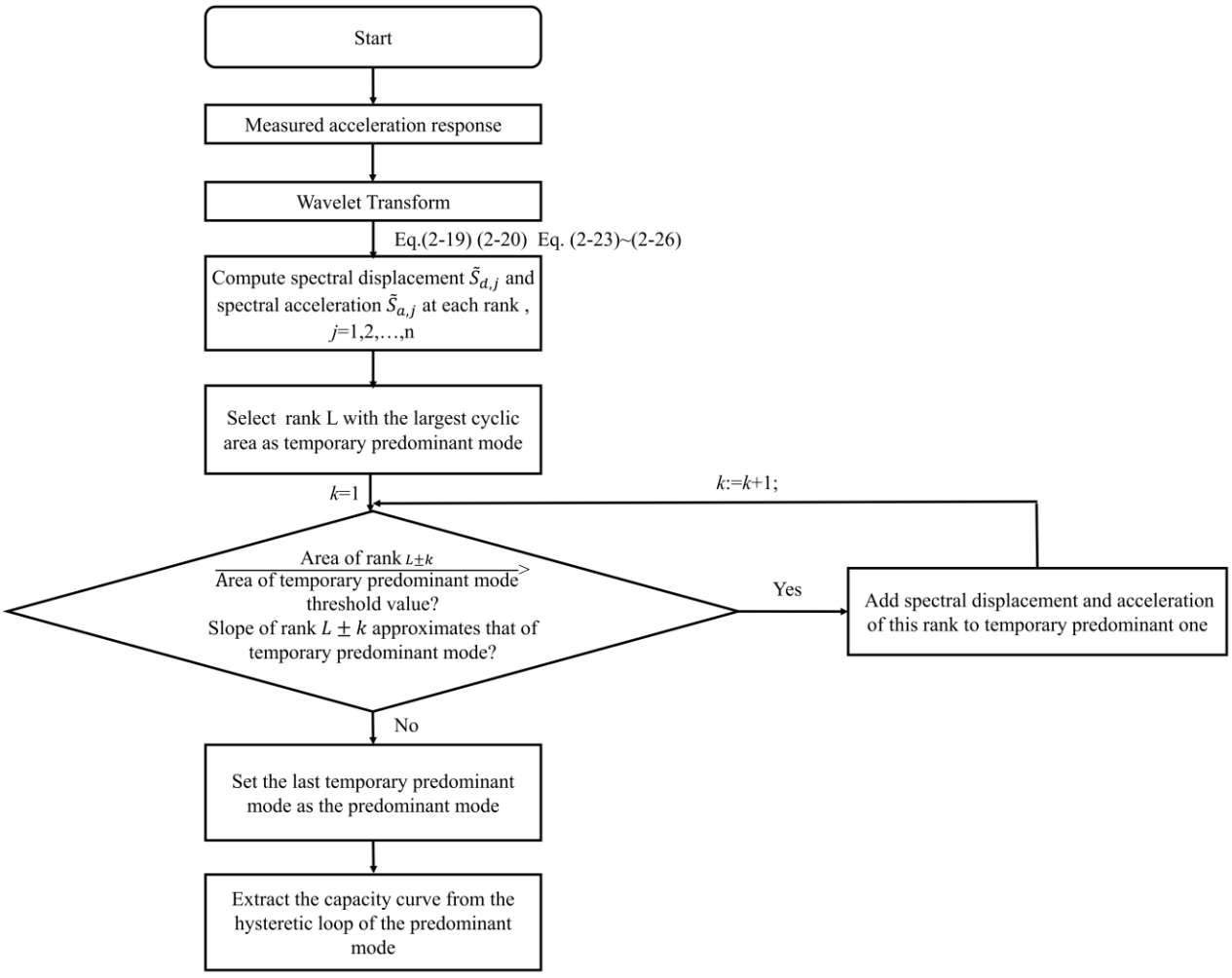

Figure 2-1 Flowchart of capacity curve estimation

2.3.3 Numerical example

In this example, performance of proposed method is presented for an elastic system. Discussion on the inelastic system will be left for section 2.4. Acceleration response was generated for 3 DOFs system subjected to a seismic wave MYG013NS observed by K-NET in Sendai on March 11, 2011 and the time history is shown in Figure 2-2. The model parameters of the system are shown in Table 2-1. The time interval used to generate the data was 0.01s and the damping ratios were set as 3% for each mode. Frequencies of the first three modes were 0.63Hz, 1.12Hz and 2.00Hz, respectively.

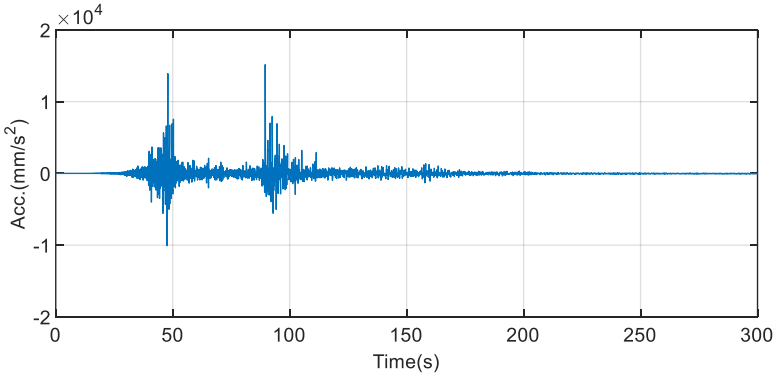

Figure 2-2 Time history of the input motion

Table 2-1 Model parameters

	Mass	Stiffness
1F	2695 kN	97.0 kN/cm
2F	540 kN	32.3 kN/cm
3F	540 kN	32.3 kN/cm

The hysteresis loops of fundamental mode estimated by proposed method are shown in Figure 2-3(a), where only Rank 7 of decomposed responses were used during calculation. Results of 6th order low pass Butterworth filters with different cutoff frequencies chosen based on visual judgement from Fourier amplitude spectrum of acceleration response are also shown in Figure 2-3(b)~(d). In each figure, the solid line denotes the hysteresis loops and the dashed line denotes the 1st mode frequency preset for model.

As shown in Figure 2-3(a), the fundamental mode is successfully extracted from measured response by the proposed method. It is clear from the figure that the response of the system is linear and the slope of the hysteresis loops agrees well with the preset value. On the other hand, the estimation result by Butterworth filtering is sensitive to the choice of cutoff frequencies where scattering is observed in some cases. It can be seen that using cutoff

frequencies of 0.8Hz can obtain the most satisfactory result among the three. However, in practice, the selection process is not readily achieved and may require manual trial and error tests.

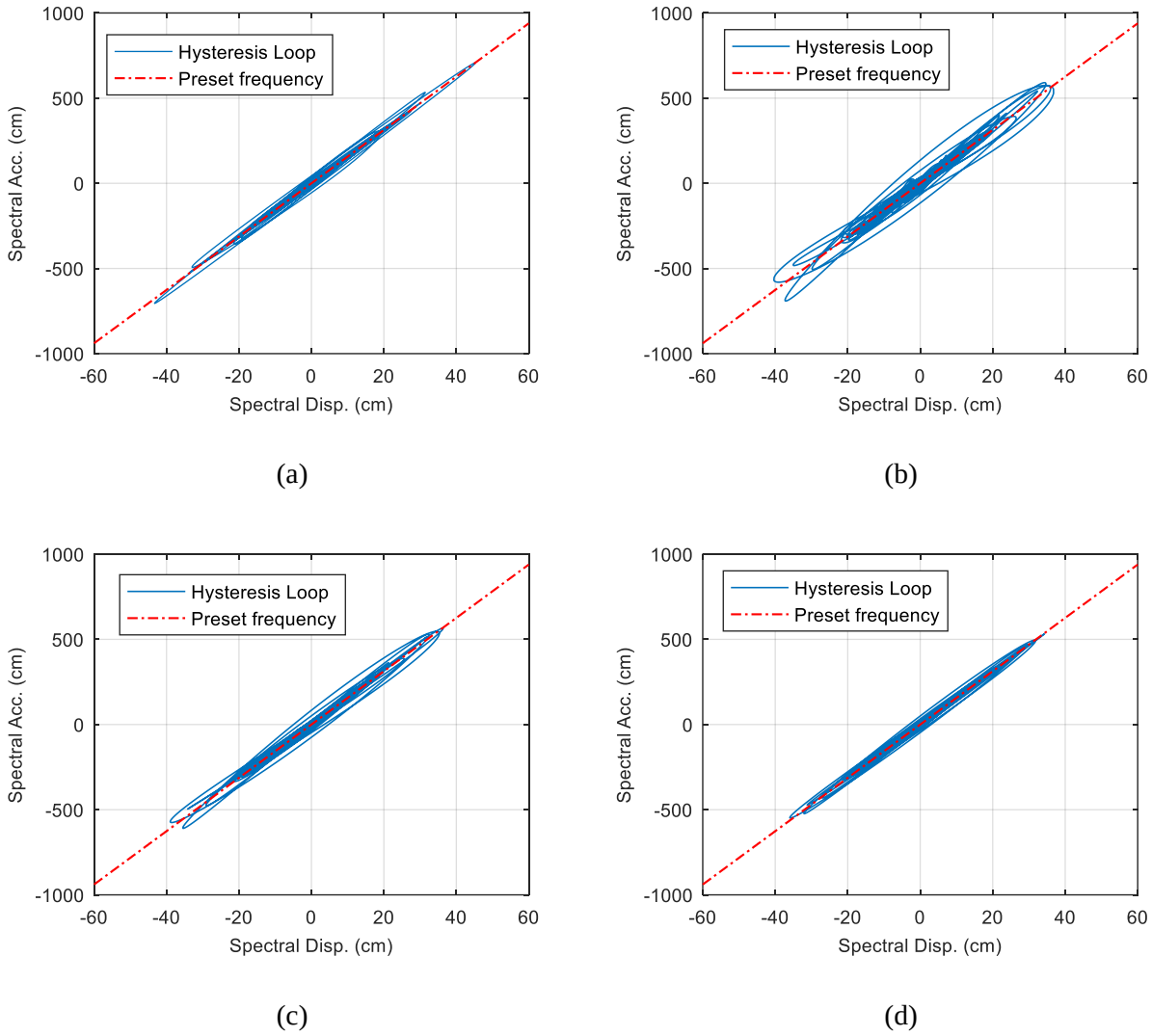

(a) (b)

(c) (d)

Figure 2-3 Hysteresis comparison (a) Proposed method using WTM (b) 1.0Hz filter (c) 0.9Hz filter (d) 0.8Hz filter

2.4. Shaking table tests

Data from a full-scale 3-story reinforced concrete frame structure shaking test [4] was utilized to validate the proposed method. The specimen had 3-story and four columns at each floor as shown in Figure 2-4. The dimensions and bar arrangements of the column and beams are listed in Table 2-2. The weight of the specimen was 37.28kN (1F), 37.07kN (2F), and 39.05kN (3F), respectively. The first three mode frequencies from the computational model by the finite element method were 3.2 Hz, 10.1 Hz and 20.1 Hz. The east-west (EW) component of the earthquake recorded at the Hachinohe station during 1968 Tokachi Oki earthquake was applied for the input motion. The input motion was scaled so that peak ground acceleration (PGA) was 6m/s2. Sampling rate of the data acquisition system was 200Hz. During the tests, yield hinges were formed at all ends of beams and bottom of the columns on the first floor.

Table 2-2 Details of members

Member	Dimension (mm)	Main bar	Hoop
Column	450×450	8-D22	D10@200mm
Beam (Roof)	250×500	Top 2-D22 Bottom 2-D16	D10@200mm
Beam (1st and 2nd floor)	300×500	Top 2-D22+1-D19 Bottom 2-D22	D10@200mm

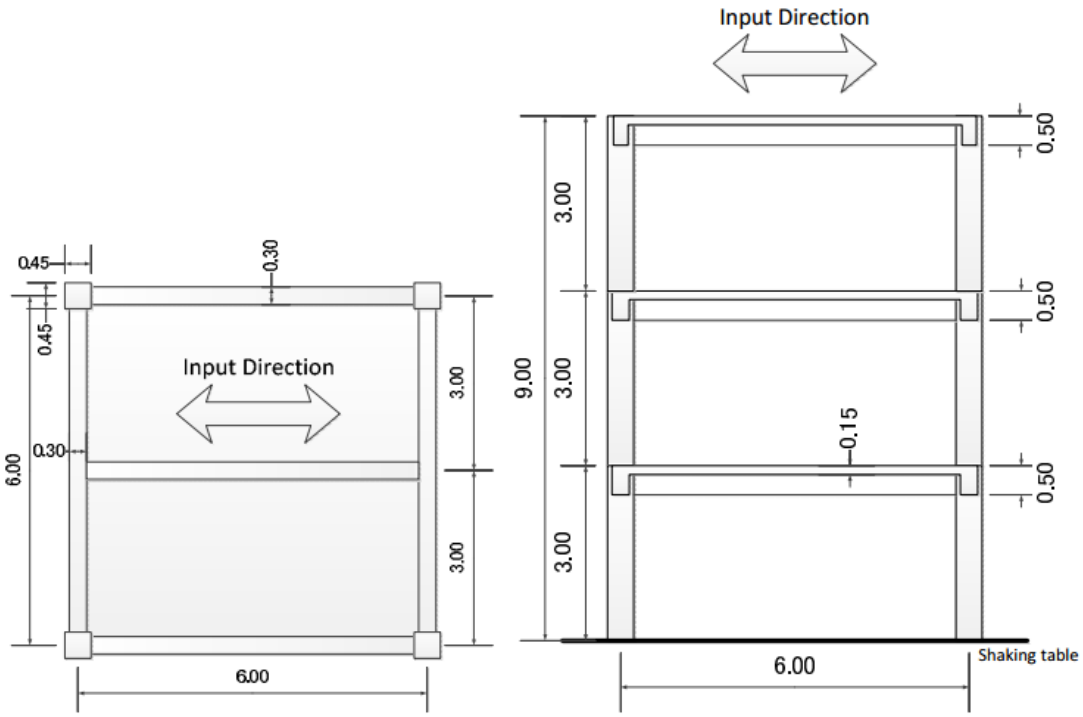

(a) Plan (b) Elevation

Figure 2-4 Dimensions of the three-story structure

Figure 2-5 shows the transfer function, i.e. the ratio of the Fourier amplitude spectrum of the top-floor acceleration to that of the ground acceleration response. It can be found that the predominant mode was obscured due to the large nonlinearity induced by the strong motion, which make it difficult to perform conventional capacity estimation methods by visual judgement based filtering.

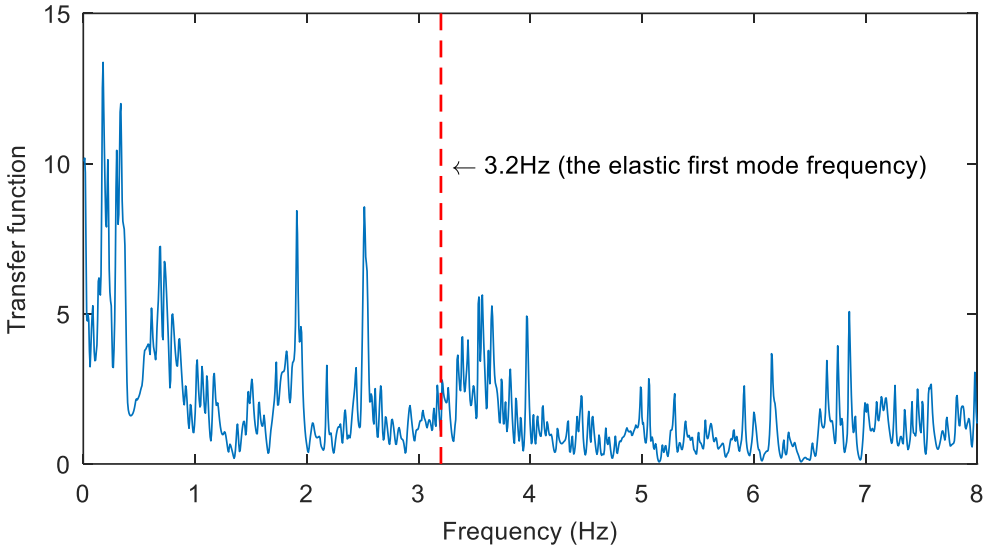

Figure 2-5 Transfer function

By utilizing WTM, the original signal was decomposed into 14 ranks. Figure 2-6 shows the hysteresis loops of each rank. Following the computation path in Figure 2-1, it turned out that Rank7 (0.78Hz~1.56Hz) had the largest area of hysteresis loops, and its adjacent rank Rank8 (0.39Hz~0.78Hz) shared a similar slope with Rank7. Finally, we set the major rank as the sum of Rank7 and Rank8, while other ranks were discarded because of too small area or inconsistent slope.

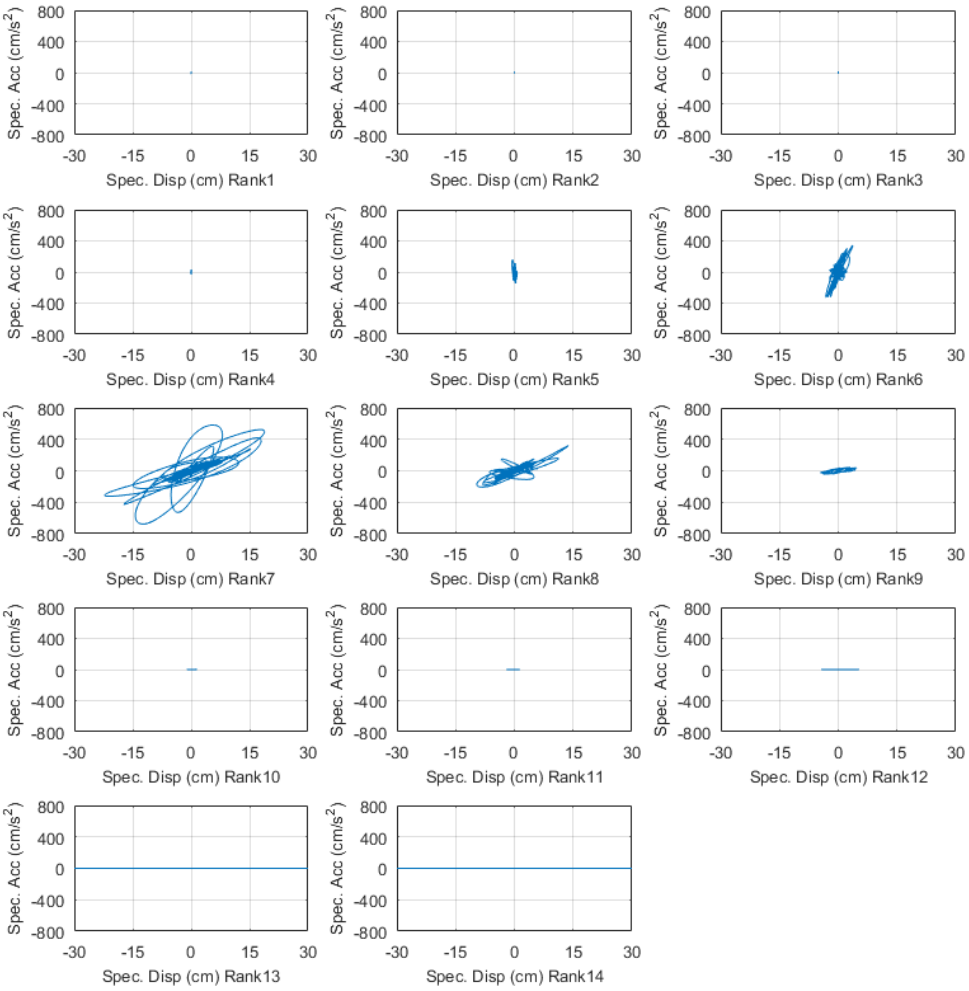

Figure 2-6 Hysteresis loops of each rank

Figure 2-7 shows the backbone curve of the capacity curve derived from hysteresis loops computed by Rank7 and Rank8. The designed fundamental frequency of 3.2 Hz is also superimposed in the figure for comparison.

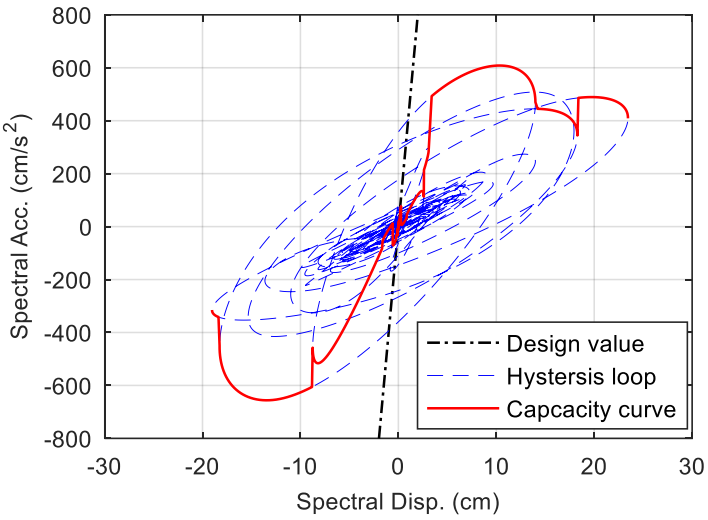

(a)

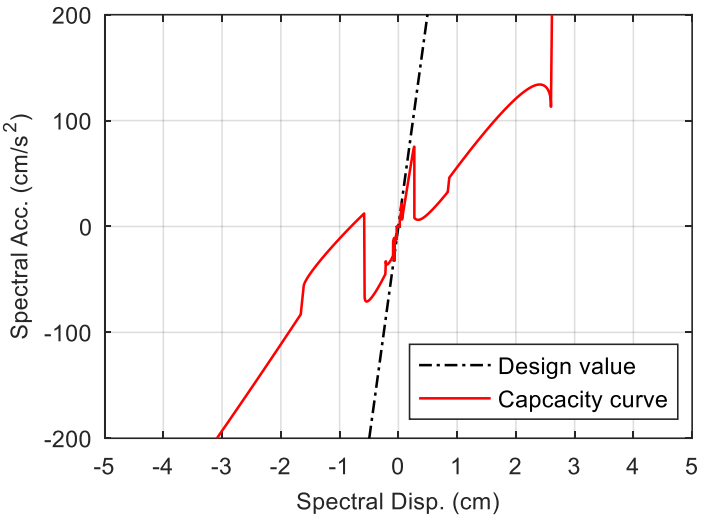

(b)

Figure 2-7 Capacity curve of the three-story structure

The nonlinear behavior of the structure is well displayed in the figure. The capacity curve shows considerable stiffness reduction during the course of the earthquake, which is consistent with the result of experiment observation. This demonstrates that the proposed method could be applied for the large nonlinear response. Next, we take a closer look in Figure 2-7(b) by zooming in Figure 2-7(a) with a focus on the linear range. The hysteresis

loops are not shown here for simplicity. It can be found that the superimposed diagonal agrees well with the estimated backbone curve in the elastic range, implying the WTM chose the first mode successfully.

2.5. Application

Having outlined the basic theory and the validation experiment of the proposed method. This section presents an example of the field application for damage evaluation using seismic response data recorded at a steel tower during 2016 Fukushima earthquake.

Hazawa Tower (Figure 2-8(a)) is located in Yokohama, Japan. This cylinder type steel tower is about 58 m from the ground and is used for micro-wave telecommunication. Tri-axial accelerometers (ITK-002, shown in Figure 2-8(b)) were instrumented at the basement, top, 1/3 and 2/3 of the total height as shown in Figure 2-8(a) with sampling rate of 100Hz.

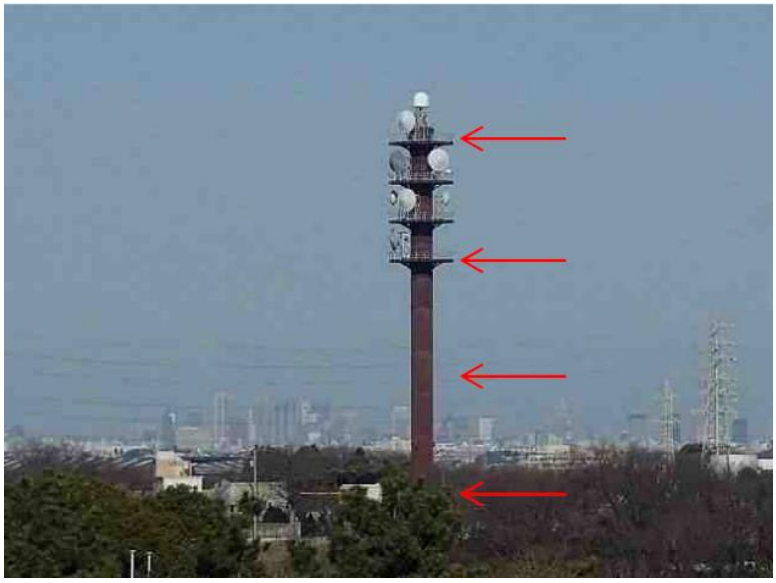

(a) Hazawa Tower

(a) ITK-002

Figure 2-8 Instrumented tower and sensor

Strong motions with magnitude 7.4 occurred at 30km beneath the seafloor of offshore of Fukushima at 5:59 am (JST) of November 22nd, 2016. The epicenter of the main shock and the location of the tower are shown in Figure 2-9. Figure 2-10 and Figure 2-11show the measured acceleration time histories and the corresponding transfer function at Hazawa Tower in northeast (NS) Direction, respectively.

Figure 2-9 Epicenter of the earthquake and sites (Map data: Google, ZENRIN)

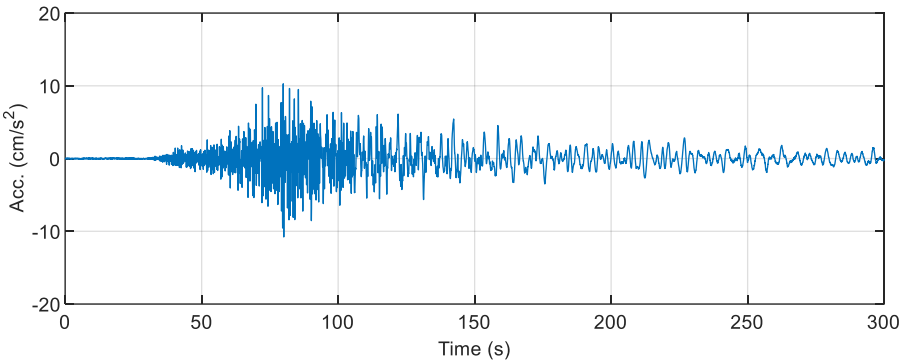

(a)

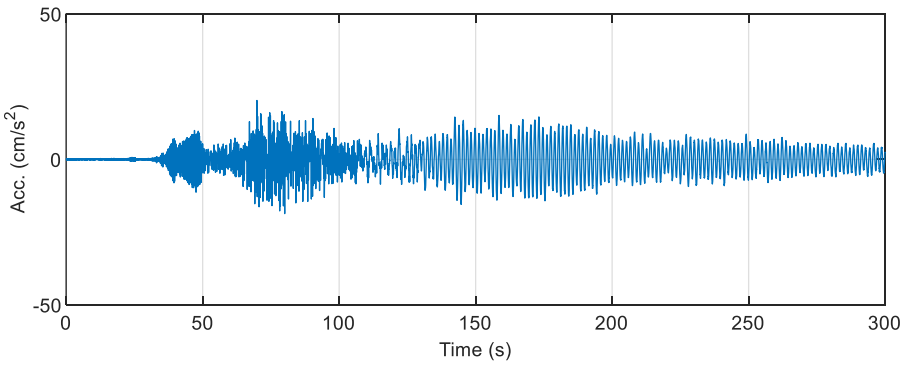

(b)

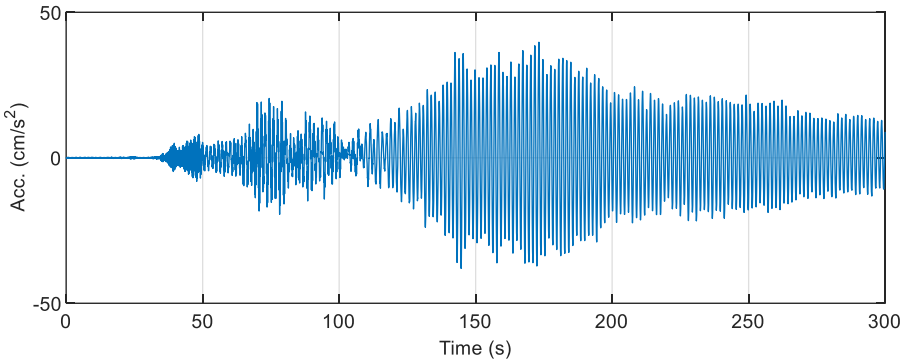

(c)

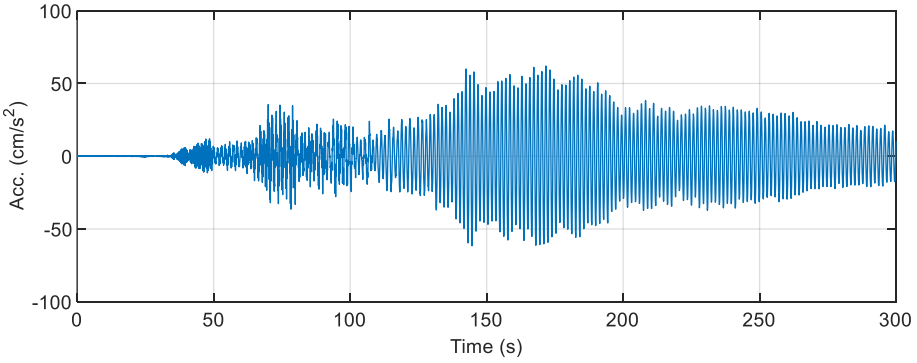

(d)

Figure 2-10 From top to bottom (ground (a), 1/3 height (b), 2/3 height (c), top of the tower (d)): Measured acceleration at Hazawa Tower in NS Direction

Capacity curve was estimated using the measured accelerations. Rank 7 (0.39Hz~0.78 Hz) and Rank 8 (0.19Hz~0.39Hz) were selected as the 1st mode component. The calculated capacity curve of Hazawa tower during Fukushima earthquake is shown in Figure 2-12. It is shown clearly that Hazawa tower remained in elastic under Fukushima earthquake. The predominant frequency derived from the capacity curve by using linear curve fitting is 0.69Hz, which is consistent with the value from the transfer function in Figure 2-11. This indicates that the number of the sensor of 3 can give a good accuracy for Hazawa tower.

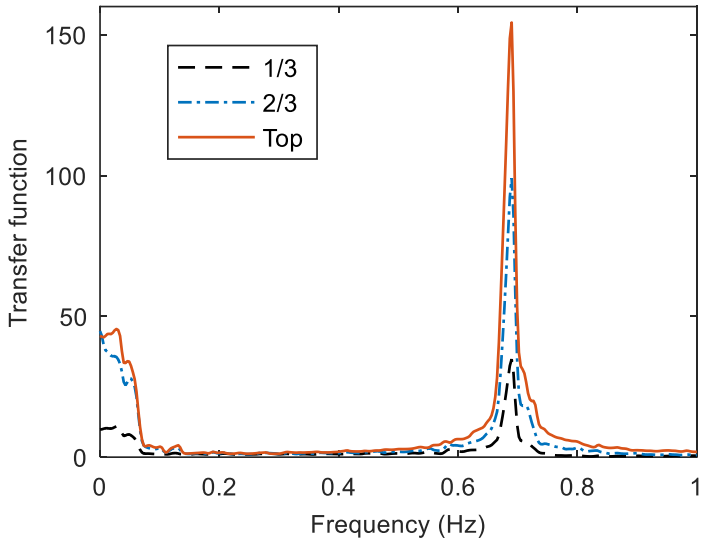

Figure 2-11 Transfer functions (NS Direction)

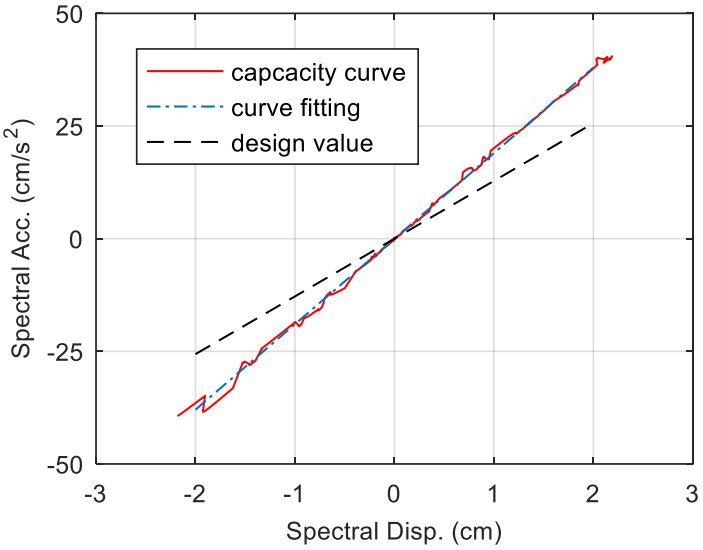

Figure 2-12 Capacity curve of Hazawa Tower

For comparison, the design predominant frequency of 0.57Hz is also shown in the figure. The measured frequency was a little larger than the design value. This finding is consistent with the results in literature review, which may be attributed to the overestimation of effective mass values at the design stage[5][6][7].

2.6. Conclusions

A novel procedure for deriving structural capacity curve from its earthquake acceleration response was presented. A clear advantage of this method is that it frees one from choosing cutoff frequencies manually and is capable of generation of capacity curve in a relatively short time. Structural damage or a change in system stiffness can be well displayed through a simplified force-displacement relationship. The feasibility of the proposed method is demonstrated by numerical examples, shaking table tests and actual recorded data of a steel tower during an earthquake event.

2.7. References

[1] Addison, Paul S. *The illustrated wavelet transform handbook: introductory theory and applications in science, engineering, medicine and finance*. CRC press, 2017.

[2] Darragh, B., W. A. L. T. Silva, and N. I. C. K. Gregor. "Strong motion record processing for the PEER center." *Proceedings of COSMOS Invited Workshop on Strong-Motion Record Processing, Richmond, Calif, USA*. 2004.

[3] Satake, Naoki, et al. "Damping evaluation using full-scale data of buildings in Japan." *Journal of structural engineering* 129.4 (2003): 470-477.

[4] Onoguchi Masami, Miyashita Shin-ichi, Kusu Koichi, Nakano Yoshiaki. Shaking Table Tests of Full-Scale Reinforced Concrete Three-Story Frame Structure : Part1 Object and Outline of Specimen. *Summaries of technical papers of Annual Meeting Architectural Institute of Japan. C-2, Structures IV*. (1995): 707-708 (in Japanese)

[5] Li, Q. S., Y. Q. Xiao, and C. K. Wong. "Full-scale monitoring of typhoon effects on super tall buildings." *Journal of Fluids and Structures* 20.5 (2005): 697-717.

[6] Li, Q. S., et al. "Dynamic behavior of Taipei 101 tower: field measurement and numerical analysis." *Journal of Structural Engineering* 137.1 (2010): 143-155.

[7] Pan, Haoran, et al. "Wind effects on Shenzhen Zhuoyue Century Center: Field measurement and wind tunnel test." *The Structural Design of Tall and Special Buildings* 26.13 (2017): e1376.

Chapter 3. Capacity curve estimation for high-rise buildings using limited number of sensors

This chapter is reproduced from the journal paper titled “Capacity curve estimation for high-rise buildings using limited number of sensors” coauthored with Koichi Kusunoki, which has been accepted by *Journal of Earthquake Engineering*, (DOI: 10.1080/13632469.2019.1592792).

3.1. Overview

In this chapter, a strategy to estimate capacity curve with a limited number of sensors for high-rise buildings based on the piece-wise cubic polynomial interpolation (PWCPI) procedure is proposed. The PWCPI procedure for interpolation is adopted here but not the mode-based procedure proposed by Goel (2008) [1] is mainly because during the process of interpolation, the mode-based procedure usually requires the model properties information, such as the distribution of stiffness, which is usually unavailable in the practice of health monitoring. On the other hand, PWCPI procedure does not need such information and is easy to implement. Meanwhile, sensors are instrumented on floors at a regular interval along the height of the building; thus, detailed structural information is not necessary for the optimization of the sensor location. Numerical simulations and shaking table tests are conducted to illustrate the method. This chapter has a narrow focus on regular buildings, where the stiffness distribution is assumed to be smoothly increased along the height of the building.

3.2. Piece-wise cubic polynomial interpolation procedure

Consider that an *N*-story building is instrumented at *J* locations including accelerometers at the ground floor and the roof. Let $Acc(h_j)$ be the acceleration measured by the *j*-th sensor located at height h_j from the ground. At a given height $h \in [h_j, h_{j+1}]$, the desired acceleration is given by

$$Acc(h) = a_j(h-h_j)^3 + b_j(h-h_j)^2 + c_j(h-h_j) + d_j \quad (3\text{-}1)$$

where a_j, b_j, c_j, and d_j are the coefficients to be estimated in each subinterval $[h_j, h_{j+1}]$. As there are $J-1$ subintervals divided by *J* sensors, $4(J-1)$ constants are needed to define the response of the building. In addition, $2(J-1)$ equations are found by matching the response at the two ends of $J-1$ subintervals, and the remaining constraints $2(J-1)$ can be given by the continuity conditions at $J-2$ junctions of the $J-1$ subintervals and the boundary conditions of the building. Interested readers can refer to Goel (2008) [1]for a more detailed description of the PWCPI procedure. In this study, cubic interpolation was performed using the MATLAB function “spline”[2].

The strategy to estimate capacity curve with a limited number of sensors can be divided into two steps. First, the accelerations of noninstrumented floors are calculated by interpolating the accelerations at floors at a regular interval along the height of the building. It is useful to emphasize that the accelerations at the base and roof of the building are always included in the interpolation. Next, the capacity curve is estimated from the accelerations at each floor using the method proposed in Chapter 2. Figure 3-1 summarizes the process.

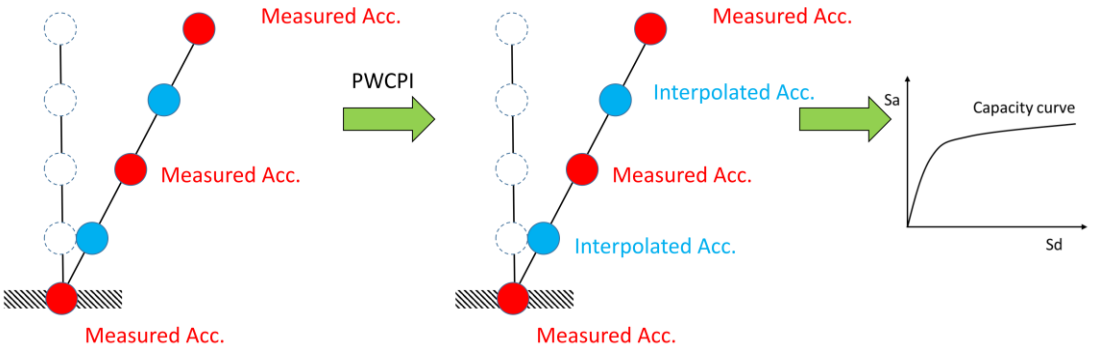

Figure 3-1 Procedure to estimate capacity curve with accelerations from limited sensors

3.3. Numerical simulation

In this section, the responses of shear buildings with 8, 18, and 28 stories subjected to seismic ground motion are used to explore the accuracy of estimated capacity curve with different number of sensors placed at regular intervals along the height of the building.

Each building was assumed to have a uniform floor mass of 200 tons. Trilinear model was used to idealize the nonlinear behavior of each story, and initial stiffness decreased with the floor height in accordance with the Japanese code [3]. The fundamental mode frequencies of the three building models were 1.639 Hz, 0.874 Hz, and 0.567 Hz, respectively. The damping was defined as classical damping with damping ratios in the fundamental and second modes to be 5%.

In this study, the accelerations at each floor were simulated by the time history analysis (THA) of building models subjected to ground motions at the base of the buildings. The motions used in the investigation are translations recorded during the 1940 Imperial Valley earthquake (Figure 3-2(a)), 1994 Northridge earthquake (Figure 3-2(b)), and 1995 Kobe earthquake (Figure 3-2(c)). The THA accelerations at limited floors were used to interpolate accelerations at the remaining floors. Next, the capacity curve was estimated

from accelerations at all floors. The accuracy of the interpolation procedure was evaluated by comparing the capacity curve from responses at all floors with that from the PWCPI procedure using responses interpolated at limited floors.

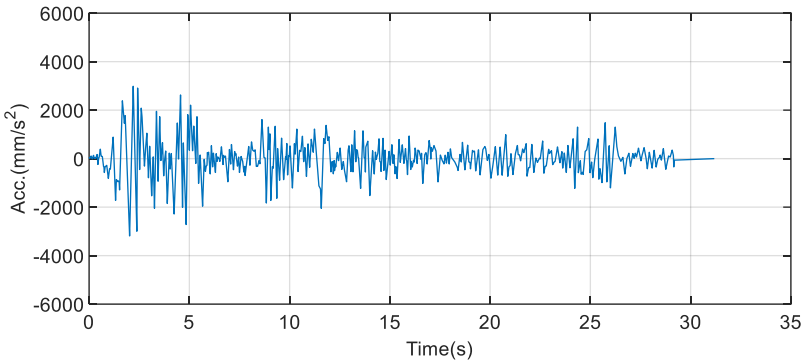

(a)

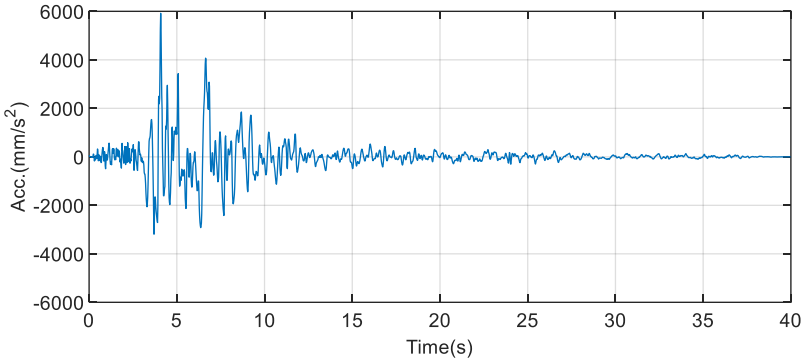

(b)

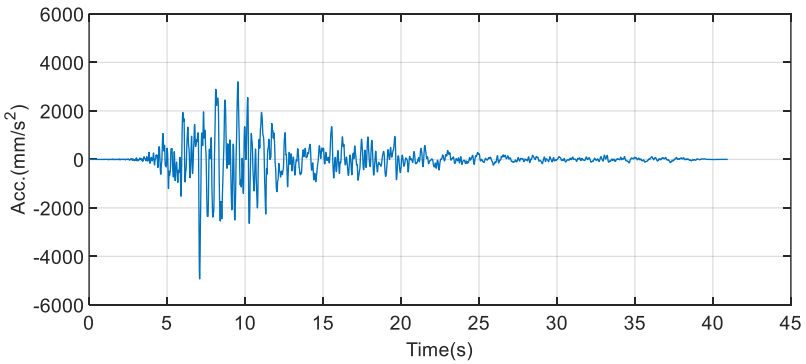

(c)

Figure 3-2 Time histories of earthquake events at 100% shaking intensity (a) 1940 Imperial Valley earthquake (b) 1994 Northridge earthquake (c) 1995 Kobe earthquake

The accuracy of the estimated capacity curve from the PWCPI procedure is defined by function of fitness F as follows:

$$F = \frac{\frac{S^{\text{Inp}}_{\text{disp.Pos}}}{S_{\text{disp.Pos}}} + \frac{S^{\text{Inp}}_{\text{disp.Neg}}}{S_{\text{disp.Neg}}} + \frac{S^{\text{Inp}}_{\text{acc.Pos}}}{S_{\text{acc.Pos}}} + \frac{S^{\text{Inp}}_{\text{acc.Neg}}}{S_{\text{acc.Neg}}}}{4} \tag{3-2}$$

where $S_{\text{disp.Pos}}$ and $S_{\text{disp.Neg}}$ are the maximum spectral displacements of the capacity curve estimated from responses at all floors without interpolation in the positive and negative directions, respectively; $S_{\text{acc.Pos}}$ and $S_{\text{acc.Neg}}$ are the corresponding spectral accelerations; $S^{\text{Inp}}_{\text{acc.Pos}}$ and $S^{\text{Inp}}_{\text{acc.Neg}}$, and $S^{\text{Inp}}_{\text{disp.Pos}}$ and $S^{\text{Inp}}_{\text{disp.Neg}}$ are the corresponding spectral acceleration and spectral displacement estimated from responses through interpolation, respectively. The capacity curve is estimated with high quality when F is close to unity.

Each input motion was scaled to different levels of peak ground acceleration so that the building models could deform from the linear-elastic range to the nonlinear range. The trend of accuracy of the PWCPI procedure with different number of sensors was plotted with respect to the maximum inter-story drift angle, as shown in Figure 3-4 - Figure 3-6.

Note that as the soft-story condition may occur in the lower floors, resulting in stiffness discontinuity, at least one additional instrument was needed somewhere in the middle floors, apart from the ground floor and the roof. Therefore, at least three sensors were required during the interpolation process.

When the building models deformed within the elastic range (maximum inter-story angle < 1/1000 rad), F was very close to unity, indicating that the estimated capacity curves from the PWCPI procedure matched well with those from responses at all floors without interpolation. Figure 3-3(a) shows the capacity curve of 18-story building estimated from accelerations using PWCPI with three sensors and capacity curve without interpolation during the Northridge earthquake. It is found that these two capacity curves agree well. The predominant frequency from the capacity curve using PWCPI was 0.87 Hz, which is consistent with the design value. A nonlinear case with three sensors during the Kobe earthquake is also presented in Figure 3-3(b), showing good consistency between the estimated capacity curve with all sensors and limited sensors.

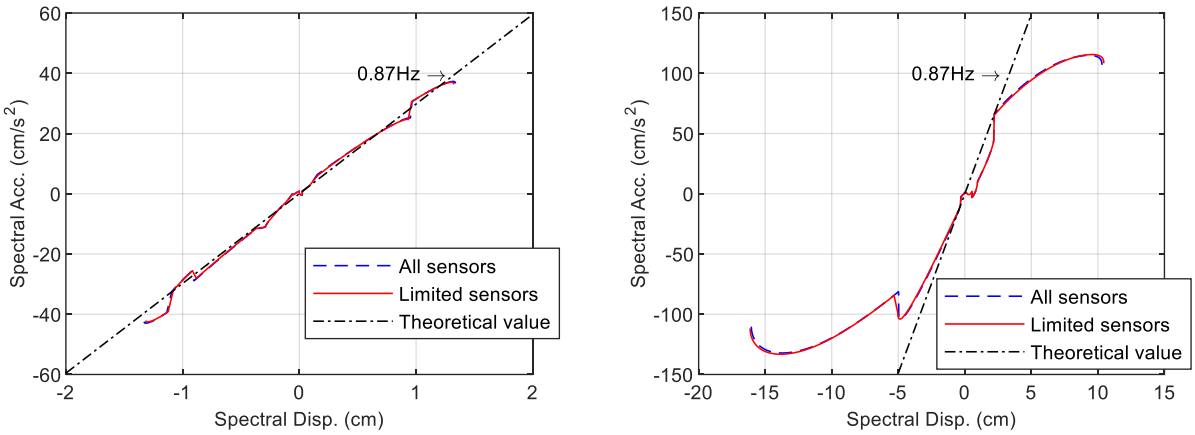

Figure 3-3 Comparison of capacity curve from THA and PWCPI: (a) linear case; (b) nonlinear case

The results presented in Figure 3-4-Figure 3-6 indicate that the accuracy was improved with increased sensors and that the accuracy was high even in a large deformation range. For the eight-story building, although there were some small fluctuations during the Kobe earthquake, F was close to unity in most cases using three sensors. Some scatters were found for the 18-story building with three sensors, and an outlier was observed at the smallest drift level when the structure behaved linearly in Figure 3-5(b). Figure 3-7 shows the capacity curve estimated at the outlier location. The capacity curve became a curve with abrupt changes. These changes resulted from inappropriate rank selection by the wavelet-based method. This shows that three sensors cannot be used to reconstruct the response and at least four sensors are necessary for the 18-story building. Four sensors are suitable for 28-story building and using more sensors could improve the accuracy. Table 3-1 summarizes the minimum number of instrumented sensors.

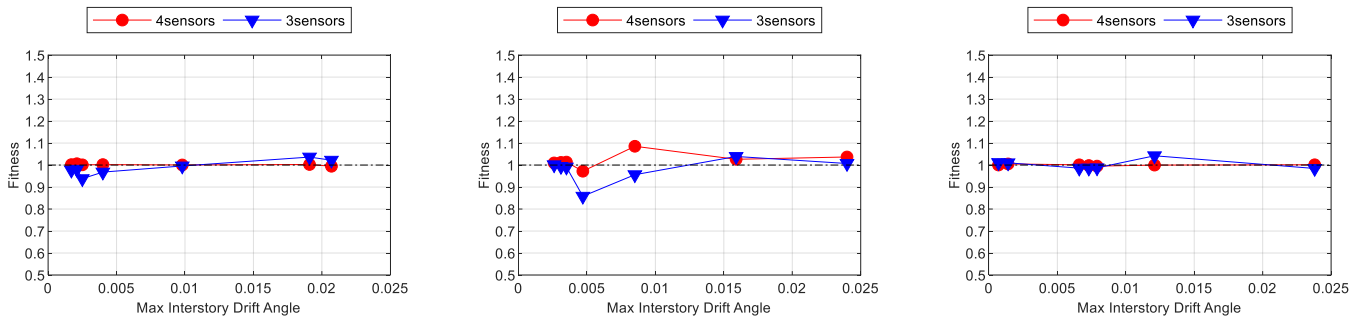

(a) (b) (c)

Figure 3-4 Accuracy of PWCPI for eight-story building during the (a) 1940 Imperial Valley earthquake, (b) 1995 Kobe earthquake, and (c) 1994 Northridge earthquake

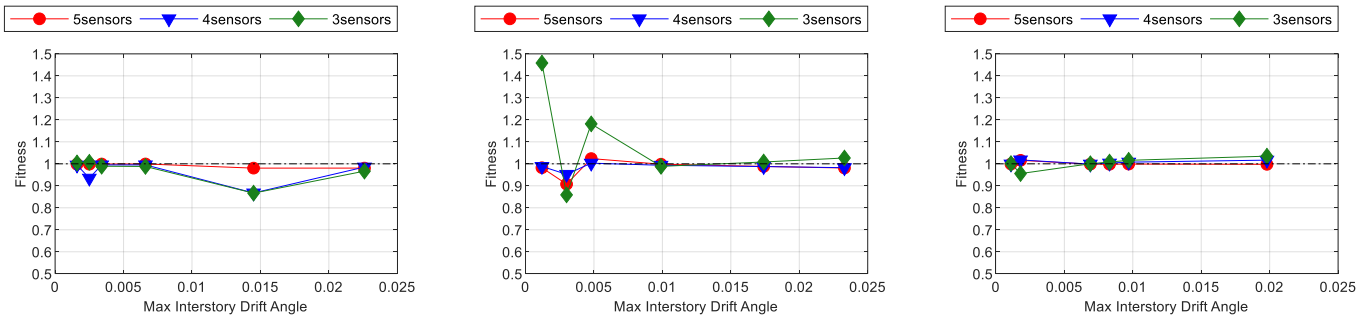

(a) (b) (c)

Figure 3-5 Accuracy of PWCPI for 18-story building during the (a) 1940 Imperial Valley earthquake, (b) 1995 Kobe earthquake, and (c) 1994 Northridge earthquake

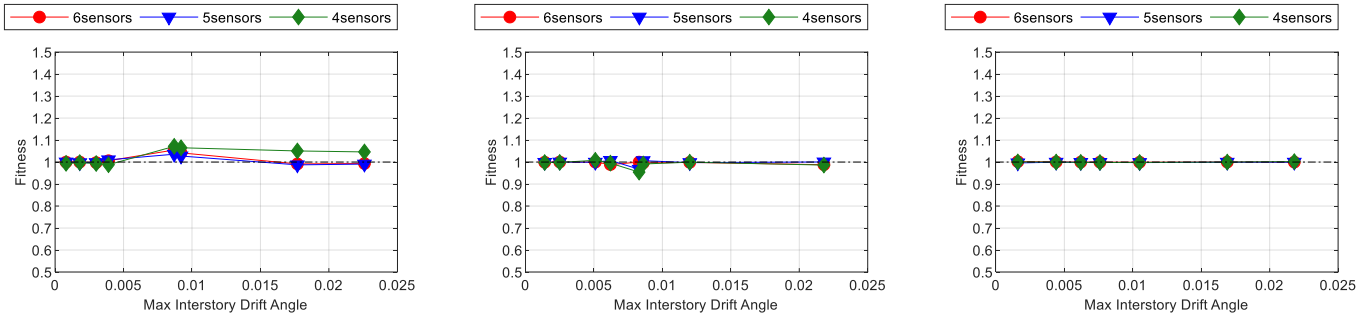

(a) (b) (c)

Figure 3-6 Accuracy of PWCPI for 28-story building during the (a) 1940 Imperial Valley earthquake, (b) 1995 Kobe earthquake, and (c) 1994 Northridge earthquake

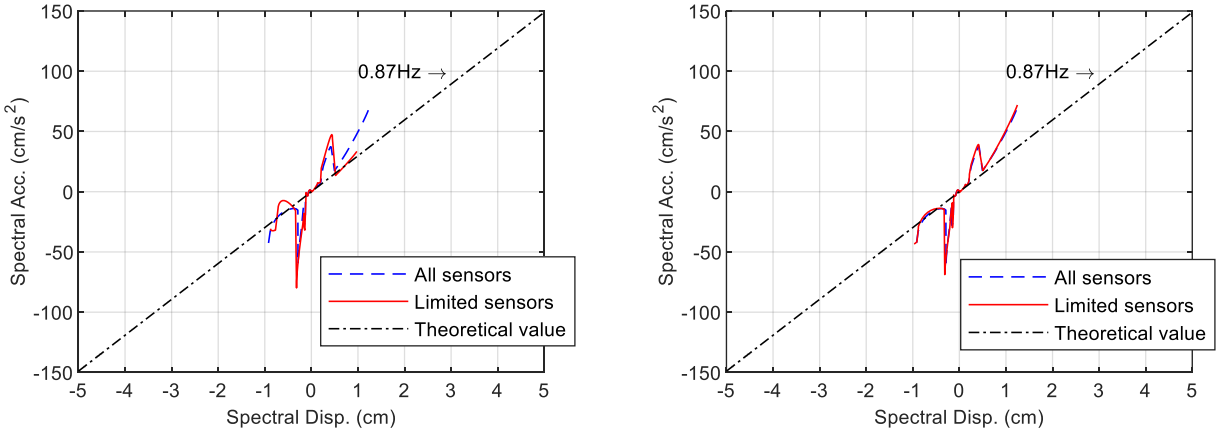

(a) (b)

Figure 3-7 Estimated capacity at the outlier location: (a) three sensors; (b) four sensors

Table 3-1 Required numbers of sensors

	8-story	18-story	28-story
Minimum numbers	3	4	4

3.4. Shaking table experiments

Having demonstrated the strategy using numerical simulations, the proposed method is applied to three shaking table experiments. These three examples deal with a 20-story reinforced concrete (RC) frame building and two six-story RC shear wall buildings with acceleration data measured during seismic excitations.

3.4.1 20-story RC frame shaking table experiment

The test structure was a 1:4 scaled model of a typical high-rise RC frame building in Japan [4] (Figure 3-9). The specimen consisted of three paralleled two-bay frames in the longitudinal direction. The story height was 0.75 m and the span widths were 1.625 m in the longitudinal and transverse directions. The model was tested on the triaxial shaking table E-defense (size: 20 m × 15 m) by exerting series of earthquake waves. Yield hinges were formed and the maximum story drift angle was 0.028 rad during the earthquakes. Figure 3-8 shows the input motion series and Figure 3-10 shows the visual inspection results of damage to the building after experiencing the earthquake series.

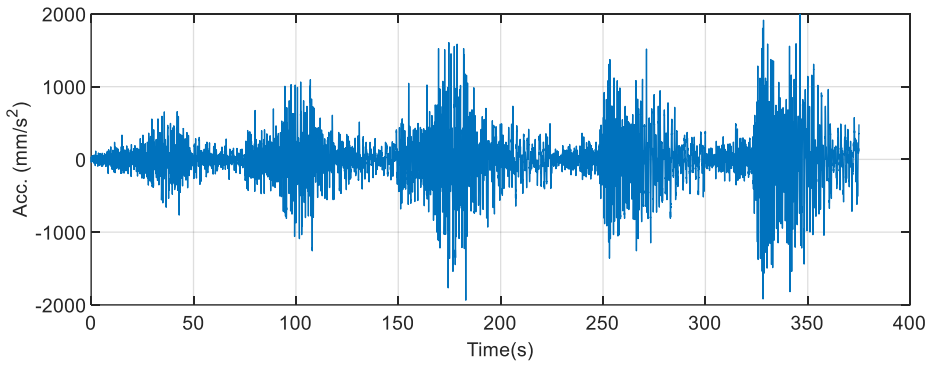

Figure 3-8 Time history of input motion series

Acceleration data used for the PWCPI procedure was utilized from sensors installed on the ground floor, 8th floor, 15th floor, and the roof, following a distribution of equal distances.

The capacity curve estimated using the PWCPI procedure was compared with that using acceleration at all floors, as shown in Figure 3-11. It can be shown that estimated capacity using data only from four sensors agrees well with that obtained using recorded data at all floors. The capacity curve in Figure 3-11 demonstrates that the stiffness of the structure decreased and the entire structure was deformed in the nonlinear range, which is consistent with the observation result of the experiment. Figure 3-12 depicts the height-wise distribution of the fundamental-mode accelerations at the peak spectral acceleration point using the PWCPI procedure and that with all sensors. This shows that the PWCPI procedure could provide good estimates of the fundamental-mode components of floor accelerations.

Figure 3-9 20-story RC frame building test model

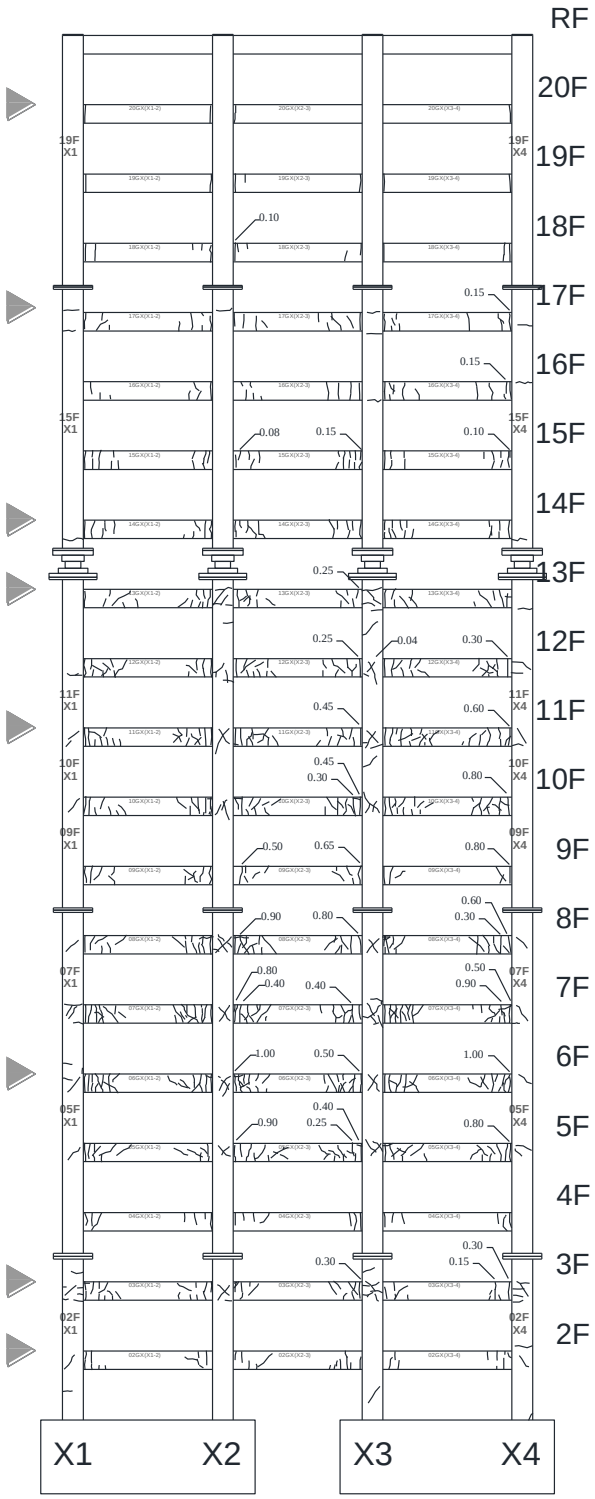

Figure 3-10 Visual inspection of damage after earthquake excitations

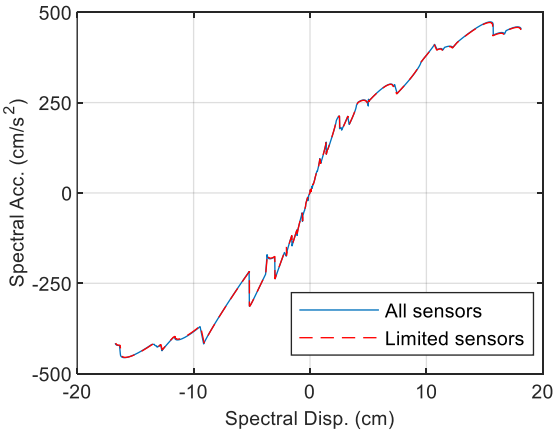

Figure 3-11 Capacity curve of 20-story building

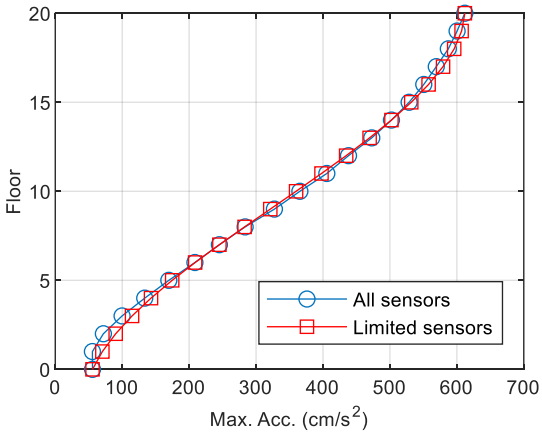

Figure 3-12 Height-wise distribution of fundamental-mode accelerations at the peak spectral acceleration point

3.4.2 Six-story RC shear wall experiment

The instrumented structure in this example was a 30%-scaled six-story RC shear wall building tested until collapse at E-defense shaking table [5] (Figure 3-14). The structure was 5.4 m long, 4.6 m wide, and 6.5 m high. Shear walls were constructed from the second to the sixth floor. The earthquake records used in the experiment were from the 1995 Kobe earthquake and were mainly applied in the transverse direction (shear wall direction) of the structure. Intensities of the ground motions were adjusted to different scale during the test. Figure 3-13 shows the time history of input motion series.

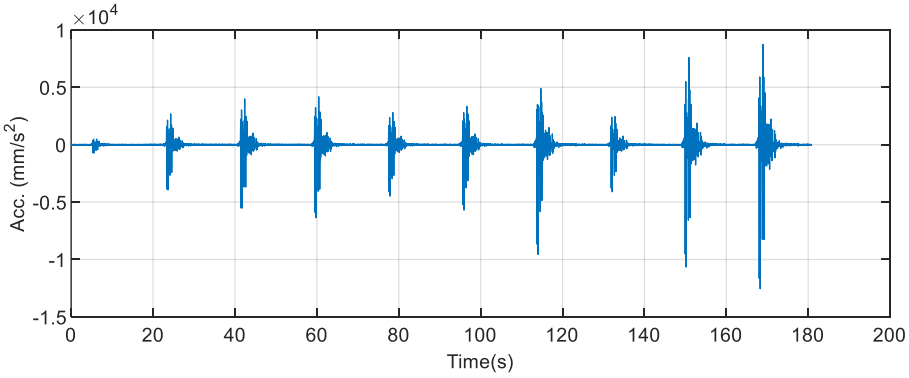

Figure 3-13 Time history of input motion series

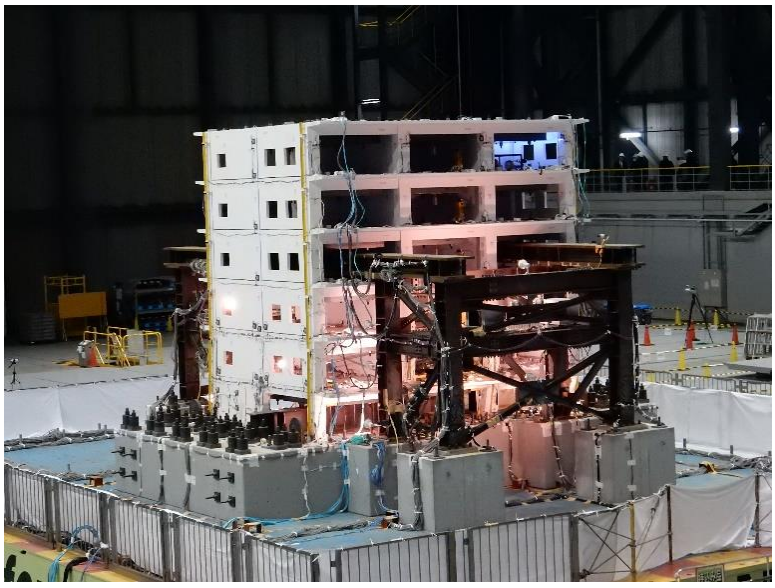

Figure 3-14 Six-story RC shear wall building test model

Figure 3-15 (a) shows the capacity curve estimated through the PWCPI procedure with three sensors installed at the ground floor, fourth floor, and the roof. Nonlinear behavior is well displayed in the figure. The spectral acceleration increases with increased spectral displacement and then begins to decrease after reaching the peak point. This phenomenon may contribute to the collapse of the structure. Although significant stiffness discontinuities may occur at the bottom of the structure when the building collapses, the capacity curve using the PWCPI procedure with three sensors and that using data from all floors was consistent. For comparison, the capacity curve estimated using PWCPI with two

sensors (ground floor and roof) is also shown in Figure 3-15 (b). These two curves matched well in the linear region, but some differences were found in the nonlinear region. Figure 3-16 (a) and Figure 3-16 (b) show the height-wise distribution of the fundamental-mode accelerations at the peak spectral acceleration point using the PWCPI procedure with three and two sensors, respectively. As shown in the figure, the height-wise distribution with three sensors approximates well with that using all sensors. Meanwhile, the error caused by using two sensors is large for the middle floors when one of the floors is ignored in the interpolation procedure and tends to be smaller for the upper and lower floors. The large error in floor accelerations results in a poor approximation of capacity curve. This implies that two sensors cannot be used to reconstruct an accurate capacity curve when the structure behaves nonlinearly. Therefore, at least three sensors are necessary in a six-story building.

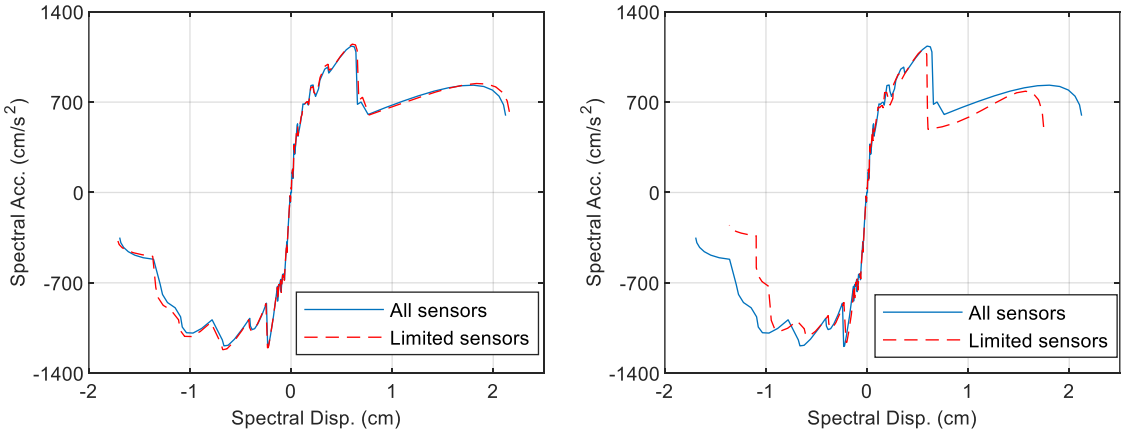

Figure 3-15 Capacity curve of six-story building: (a) three sensors; (b) two sensors

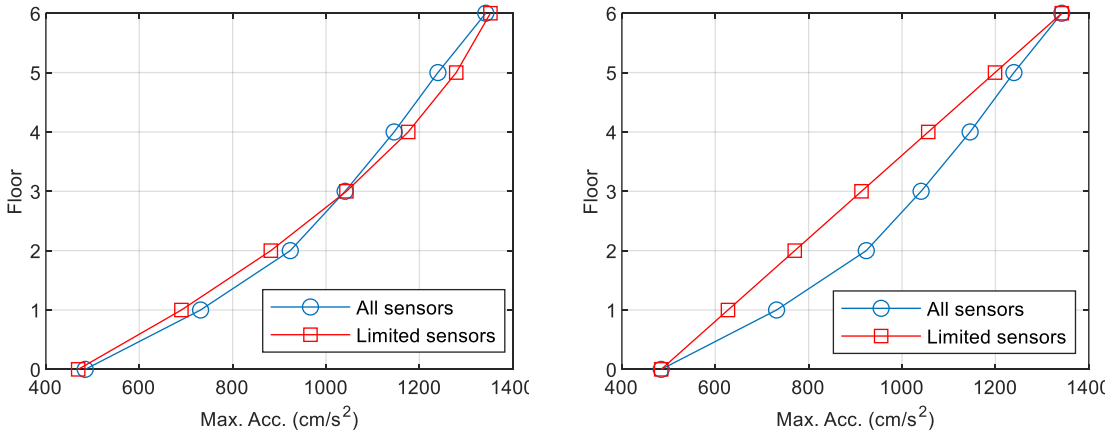

Figure 3-16 Height-wise distribution of maximum acceleration using the PWCPI procedure: (a) three sensors; (b) two sensors

3.4.3 Six-story RC shear wall experiment

This test specimen here is a 6-story shear wall RC building[6] (Figure 3-18) tested on the tri-axial shaking table E-defense (size: 20m×15m) by exerting series of earthquake waves. The input motion was the horizontal components (East-west and North-south) and the vertical (Up-down) component of the 1995 Hyogo-ken Nambu earthquake recorded at the Japan Meteorological Agency. All three components were applied simultaneously. To induce progressive damage of the structure, the specimen was subjected to a series of scaled earthquake loads during the tests. The specimen finally collapsed due to shear failure in short columns and the structural wall at the 1st-story during the last strong earthquake motion. Figure 3-17 shows the time history of the input motion series.

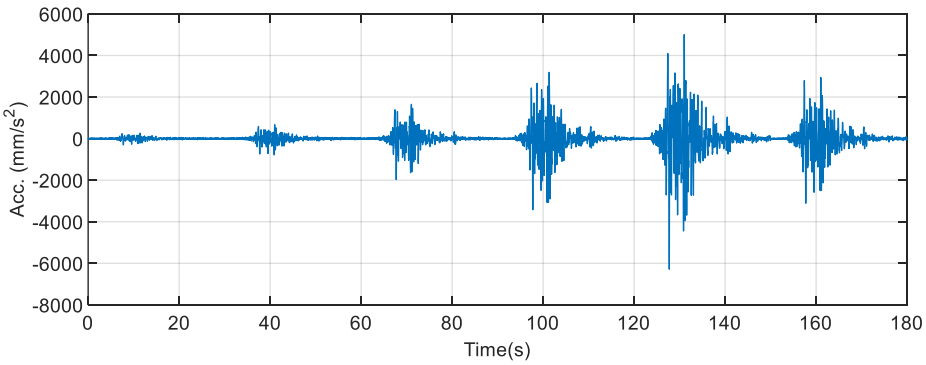

Figure 3-17 Time history of the motion series

Figure 3-18 Six-story RC shear wall building test model

Figure 3-19(a) shows the capacity curve estimated through the PWCPI procedure with three sensors installed at the ground floor, fourth floor, and the roof. The nonlinear behavior is apparent as shown in the figure. The figure also shows that the capacity curve using the PWCPI procedure with three sensors matched well with that using data from all. For comparison, the capacity curve estimated using PWCPI with two sensors (ground floor and roof) is also shown in Figure 3-16(b). Like the previous 6-story case, these two curves matched well in the linear region, but the curves in the nonlinear region show some difference. Figure 3-20(a) and Figure 3-20(b) show the height-wise distribution of the

fundamental-mode accelerations at the peak spectral acceleration point using the PWCPI procedure with three and two sensors, respectively. As shown in the figure, the height-rise distribution with three sensors approximates well with that using all sensors. However, the error caused by using two sensors is large, especially for the middle floors when one of the floors is ignored in the interpolation procedure. The large error in floor accelerations results in a poor approximation of capacity curve. This replicates the finding in the previous case. Therefore, at least three sensors are needed in a six-story building.

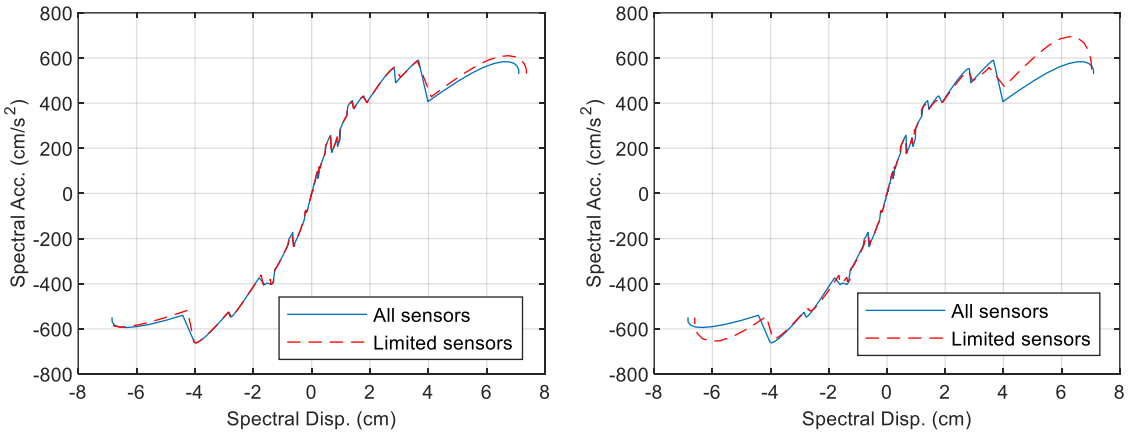

Figure 3-19 Capacity curve of six-story building: (a) three sensors; (b) two sensors

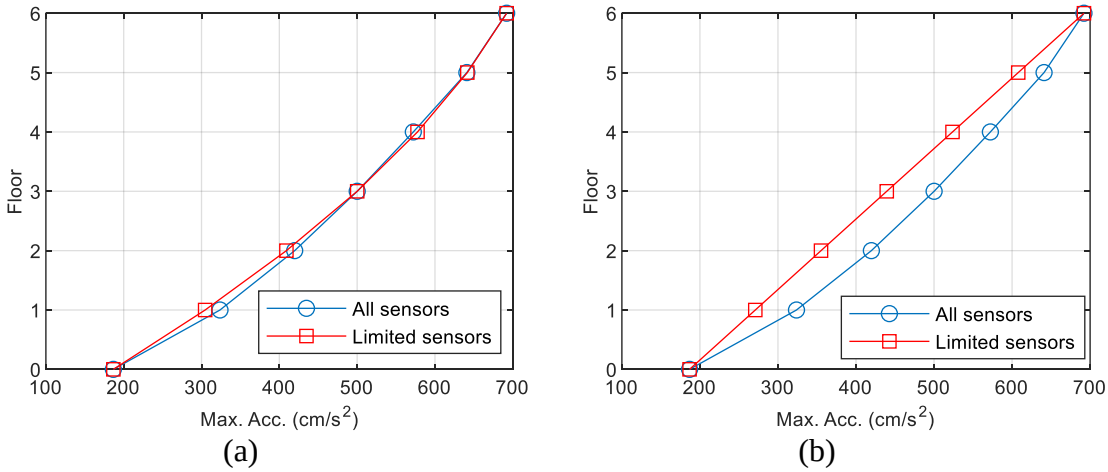

Figure 3-20 Height-wise distribution of maximum acceleration using the PWCPI procedure: (a) three sensors; (b) two sensors

3.5. Conclusions

A strategy for capacity curve estimation from accelerations at limited floors is proposed. Numerical simulations and shaking table tests have shown that the estimations based on the PWCPI procedure using data from sensors placed at regular intervals provide good estimates at the linear-elastic range as well as the nonlinear range. The entire procedure does not require sensors to be installed at optimal locations calculated from the modal property. This finding is useful and convenient in practice, because modal property, such as mode shape, is not always available for the instrumented building. The required number of sensors is also provided in this study.

3.6. References

[1] Goel, Rakesh K. "Mode-based procedure to interpolate strong motion records of instrumented buildings." *ISET Journal of Earthquake Technology* 45.3-4 (2008): 97-113.

[2] Higham, Desmond J., and Nicholas J. Higham. *MATLAB guide*. Vol. 150. Siam, 2016.

[3] Nagao, T., H. Mukai, and D. Nishikawa. "Case Studies On Performance Based Seismic Design Using Capacity Spectrum Method." *Structural Engineering Dept., Nihon Sekkei Inc., Shinjuku, Tokyo* (2000).

[4] Sugimoto, Kuniyoshi, et al. “Shaking Table Test of 1/4 scaled 20 Story RC Building under Long Period Ground Motions : Part 1: Outline of the project and test specimen.” Summaries of technical papers of Annual Meeting Architectural Institute of Japan. Structures IV (2013): 653-654 (in Japanese)

[5] Sugimoto, Kuniyoshi, et al. “Collapse behavior of 6 story wall frame building during shaking table test”. Journal of Structural and Construction Engineering (Transactions of AIJ) (2017):1759-1768 (in Japanese)

[6] Matsumori T, Shirai K, Kabeyasawa T. “Study on seismic performance of R/C wall-frame structures based on large-scale shaking table test: outline offull-scale 6-story specimen and tri-axial shaking table test.”Journal of Structural Construction Engineering (Transactions of AIJ). 2007;72:85-90. (in Japanese)

Chapter 4. Validation of post-earthquake damage evaluation using field survey results, shaking table tests and numerical simulations

4.1. Overview

This chapter will present the validation of post-earthquake damage evaluation using field survey results, shaking table tests and numerical simulations. This study will have a narrow study on RC buildings, because they are widely constructed around the world. The field survey results and shaking table tests are used for the validation of damage evaluation for mainshock, while the numerical simulations are used for aftershock, respectively. Comparisons between the result using the capacity curve method and visual inspection-based guideline for post-earthquake damage evaluation in Japan[1] are also presented.

4.2. Methodology

4.2.1 Outline of the methodology[2][3]

The framework for post-earthquake damage evaluation based on capacity curve is shown in Figure 4-1. The capacity curve here denotes the relationship between the mass-normalized base shear and roof displacement derived from the recorded accelerations of the instrumented building, in which the displacements are obtained by the double integral using a wavelet transform. The demand curve represents the demand for the structure given an earthquake, which is obtained from the ground acceleration. The demand curve with 5% viscous damping is usually adopted for elastic range. When the structural behavior is nonlinear an additional damping effect is considered. Then, the demand curve is reduced

from the 5% elastic demand curve, as shown in Figure 4-1. The intersection of the capacity curve and the reduced demand curve is the predicted maximum response during the mainshock. In practice, the maximum deformation of capacity curve estimated from measured seismic can be considered as the maximum response under the mainshock and thus demand curve is not needed.

Similarly, this method can also be extended to predict the maximum response during a MA sequence by considering the mainshock and its subsequent aftershock as a single earthquake input. Given that the input energy of the combined earthquake is greater than that of the mainshock alone, the maximum response of the former would usually be greater. One simple method of accounting for this in the capacity spectrum is to reduce the equivalent damping and the subsequent reduction in demand, as indicated in Figure 4-1. The predicted maximum response during the MA sequence is the intersection of the demand curve and the capacity curve and then the damage class can be judged.

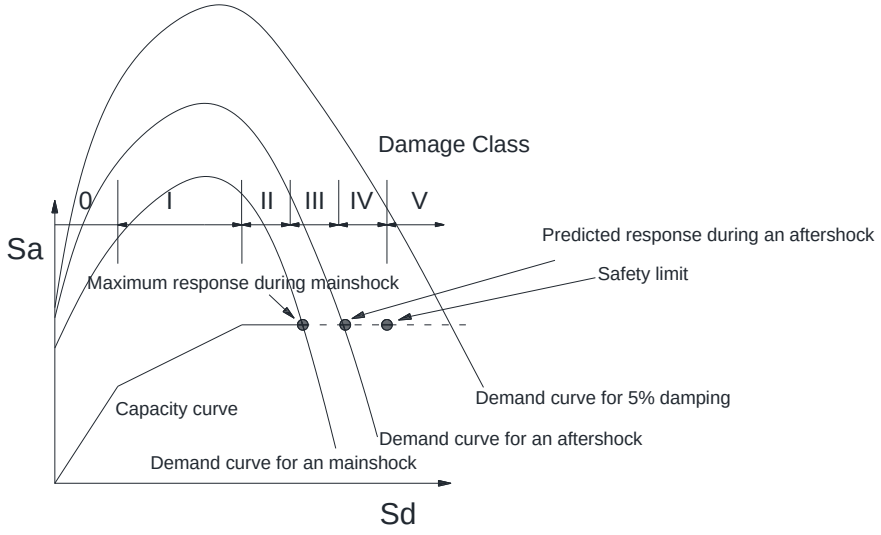

Figure 4-1 Concept of the CCB method

For the demand curve for aftershock, as specified in Japan design code [4][5],the response spectral acceleration and displacement of the demand curve for a yielding structure subjected to earthquake is reduced from the elastic demand curve with 5% damping by the response spectrum reduction factor F_h:

$$F_h = \frac{1.5}{1+10h_{\text{eq}}} \tag{4-1}$$

$$h_{\text{eq}} = \gamma(1-\frac{1}{\sqrt{\mu}}) + 0.05 \tag{4-2}$$

where μ is the ductility factor of the structure. h_{eq} is the total equivalent viscous damping and γ is the reduction factor considering the damping effect for the nonlinear seismic response of the building. For RC structures, γ usually takes the values of 0.25.

Kusunoki (2006)[6] proposed a reduction coefficient γ of 0.06 for the estimation of the equivalent damping ratio during a MA sequence through numerical study, in which the maximum aftershock is assumed to be the same as the mainshock.

To evaluate the damage state in a quantitative manner, the capacity curve obtained using measured responses is modeled as a tri-linear backbone curve here. The tri-linear curve is widely adopted in simulation of the backbone of RC structural hysteretic behaviors ([8]-[11]) for its acceptable modeling complexity and computational accuracy. The damage state of a building is classified into five classes (0: no damage I: slight, II: minor, III: moderate, IV: severe, V: collapse) in terms of the mass-normalized force-displacement relationships, which represents the structural behavior ranging from elasticity to totally collapse, as illustrated in Figure 4-1. Class 0 is the state when the structural behavior is linear and no damage occurs. Class I corresponds to a state when sporadic cracks start to occur in concrete but the reinforcement is yet to reach the yield limit. Then, if deformation exceeds the yielding point, the initiation of reinforcement would result in larger cracks in concrete, and the strain in the compressive concrete will rapidly increase to the strain at maximum stress (Class II to Class IV). Here, the region between Class II and Class IV is divided evenly for simplicity. When the deformation exceeds the safety limit state(SLS) (Class V), the lateral and vertical load sustaining capacities are lost.

The safety deformation of the entire structure can be predicted using the story deformations at the second corner and the last step of the trilinear modeled capacity curve[7]. It was found that the safety limit deformation can be predicted within 10% error when the maximum response is around the second corner point of the trilinear model, and within the few percent error when the maximum response exceeds the second corner point.). The preset limit state could be different for different structural system. In practice, it is reasonable to set the limit as the inter-story drift angle of 1/50 for RC frame building and 1/100 for RC shear wall building

4.2.2 Damage evaluation procedure

The damage evaluation strategy for RC structures is summarized as follows:

1. Estimate the capacity curve using measured seismic responses and model the restoring force characteristic by converting capacity curve into the tri-linear fitting curve.

2. For damage evaluation for mainshock, evaluate the damage class with the modeled restoring force using the damage index in section 4.2.1.

For damage prediction for aftershock, obtain the inelastic response curve for the yielding structure using the estimated response reduction calculated by Eq. (4-1) and Eq. (4-2), in which γ would be selected as 0.06. Next, evaluate the damage class using the intersection of the capacity curve and demand curve and the damage index in section 4.2.1.

4.3. Japanese guideline for damage evaluation

The damage evaluation method in the Guideline for Post-Earthquake Damage Evaluation and Rehabilitation of RC Buildings in Japan is based on the residual seismic capacity ratio index *R*, which is defined to represent the residual seismic performance of earthquake-damage buildings.

The *R*-index for each direction in each story of the target building is defined by Eq. (4-3) based on the damage condition of each column of that floor, which is calculated based on the seismic capacity reduction factor η listed in Table 4-1. η is defined as the ratio of the residual energy dissipation capacity to the original energy dissipation capacity of the member, as illustrated in Figure 4-2.

$$R = \frac{\sum_{j=0}^{V} \eta_j \cdot n_j}{\sum_{j=0}^{V} n_j} \times 100(\%) \qquad (4\text{-}3)$$

where j is the damage class of the column in Table 4-1; η_j is the seismic capacity reduction factor for the columns with damage class j; and n_j is the number of the columns with damage class j.

The damage levels of a structure can be evaluated based on the R index.

[slight damage] $R \geq 95\%$

[Minor damage] $80 \leq R < 95\%$

[Moderate damage] $60 \leq R < 80\%$

[Severe damage] $R < 60\%$

[Collapse] $R \approx 0$

Table 4-1 Damage class definition with the seismic capacity reduction factor η for ductile reinforced concrete columns

Damage class, j	Description of damage	η_j
0	No damage	1.0
I	Visible narrow cracks on the concrete surface	0.95
II	Visible clear cracks on the concrete surface	0.75
III	Local crush of cover concrete	0.5
IV	Significant crush of concrete with reinforcing bar exposure; Spalling of concrete cover	0.1
V	Buckling of the reinforcing bars; Significant damage to the core concrete; Visible vertical and/or lateral deformation of the column; Visible settlement and/or leaning of the building	0

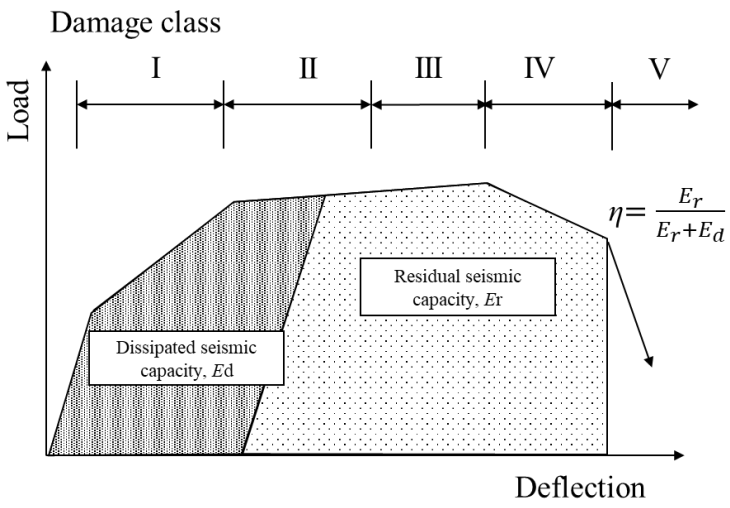

Figure 4-2 Definition of the seismic capacity reduction factor η

4.4. Investigation of capacity-curve-based method

4.4.1 Field survey

The department building of architecture, Yokohama National University is a reinforced concrete building located in Yokohama, Japan. The height of the building is 30.8m with 8 stories and 1 underground floor (Figure 4-4). Tri-axial accelerometers have been installed on every floor of the building since 2008, and the monitoring system functioned well during the 2011 Tohoku earthquake. Figure 4-3(a) and (b) give the measured accelerations of the basement and the roof, respectively.

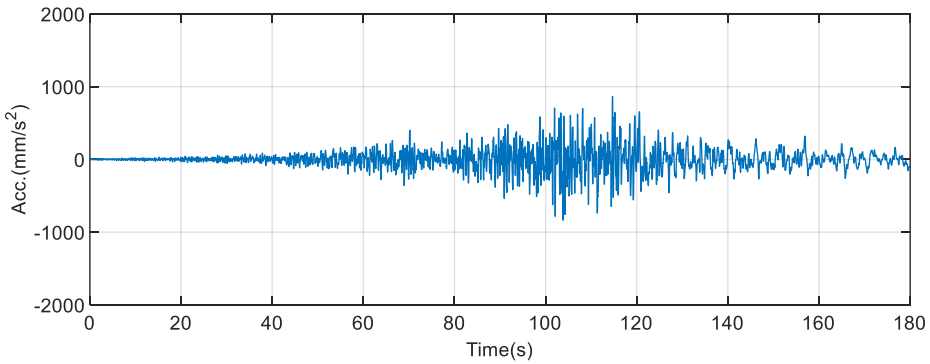

(a)

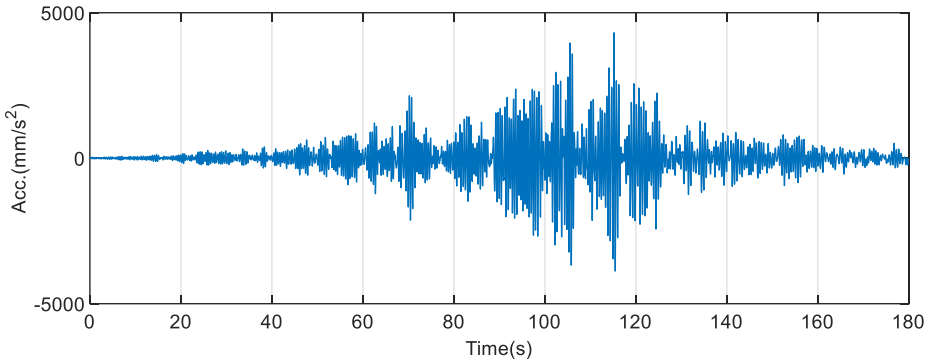

(b)

Figure 4-3 Time histories of measure accelerations (a) Basement (b) Roof

(a)

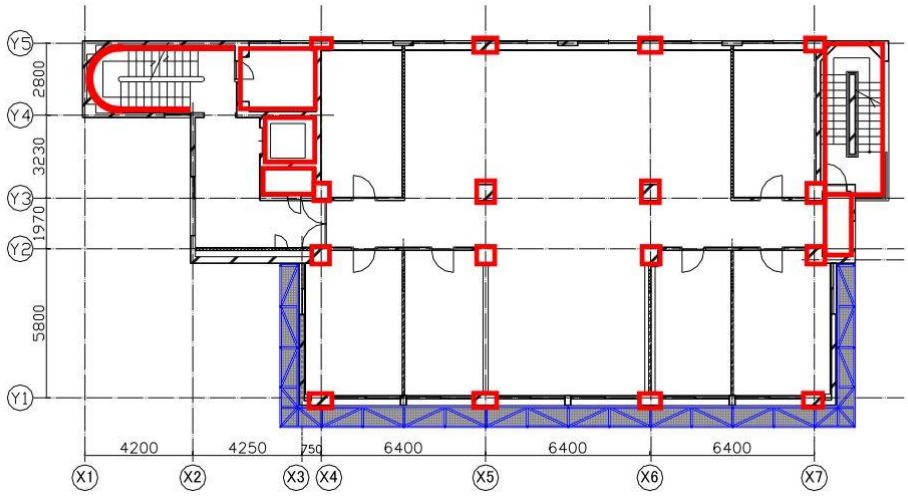

(b)

Figure 4-4 (a) The instrumented building (b) the key plan

The capacity curve is successfully estimated from measured accelerations of the basement and of each story of the building during the main shock, as shown in Figure 4-5. Restoring force characteristic modeling is performed on the estimated capacity curve. It can be shown that cracking takes place and the whole structure begins to deform into the inelastic range.

From the modeled capacity curve, the damage class of the building is evaluated as I, minor damaged (Figure 4-5(a)). Field surveys were also conducted after the main shock. As shown in Figure 4-5(b), small cracks were found mainly at the bottom of the continuous shear walls and at the corner of openings, which indicated the building had suffered minor damage. These results are consistent with the one made by the CCB method.

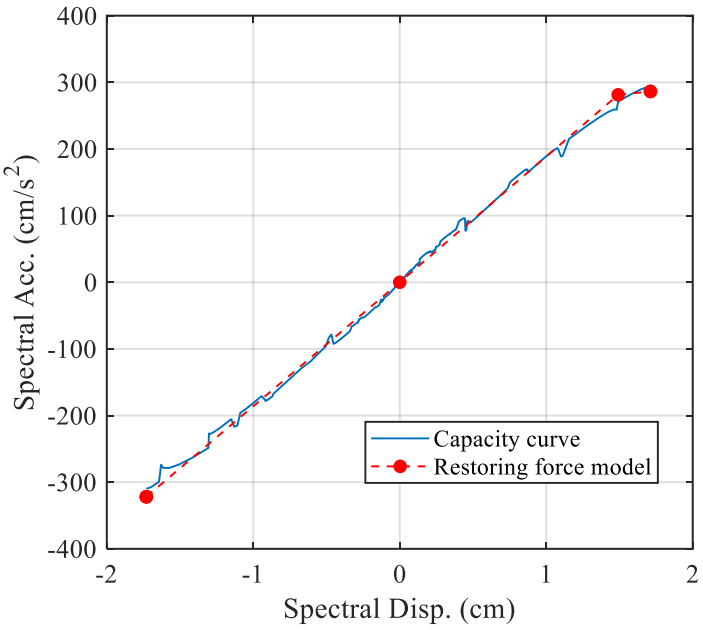

(a)

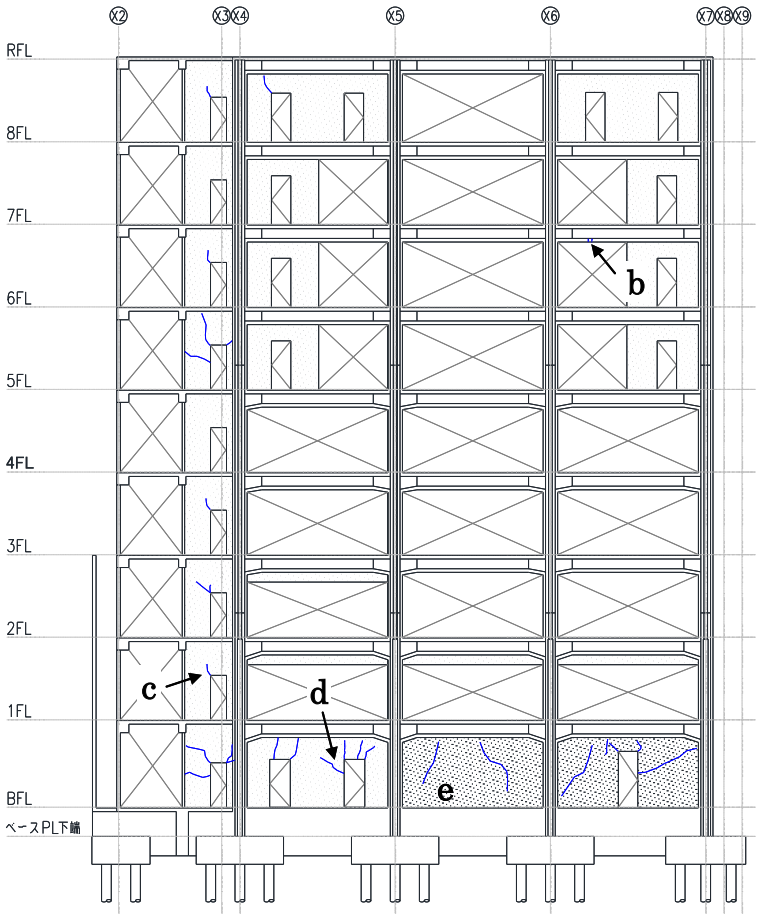

(b)

Figure 4-5 Comparison between the capacity curve and the field survey (a) Capacity curve during 2011 Tohoku earthquake (EW direction) (b) Observed cracks in the EW direction

4.4.2 Shaking table tests

This section presents an experimental investigation of seismic damage evaluation of a full scale 6-story RC wall-frame building model (Figure 4-6)using the CCB method. An outline of the shaking table tests is given here, and a more detailed description can be found in [12]. The test specimen consisted of 3 paralleled three-bay in the longitudinal (*Y*) direction and two bays in the transverse (*X*) direction. The span widths were 5 m in the longitudinal and transverse direction. The plan dimensions were 15m by 10m, and the height of the

structure was 15m. The central frame had a structural wall in the central bay continuously from the 1st to the 6th story.

The model was tested on the tri-axial shaking table E-defense (size: 20m×15m) by exerting series of earthquake waves. The input motion was the horizontal components (East-west and North-south) and the vertical (Up-down) component of the 1995 Hyogo-ken Nambu earthquake recorded at the Japan Meteorological Agency. All three components were applied simultaneously. To induce progressive damage of the structure, the specimen was subjected to a series of scaled earthquake (Table 4-2) loads during the tests. The specimen finally collapsed due to shear failure in short columns and the structural wall at the 1st-story during the last strong earthquake motion. Table 4-3 gives the damage observations and the maximum story drift angle for the 2nd story.

Damage evaluations were conducted with the capacity-curve-based method at the end of each input motion. These evaluations included the building response from proceeding excitations. For example, the evaluation for Input 3 would also consider the building response under Input 1 and Input 2. This is to ensure that cumulative damage effects are considered in the assessment. Figure 4-7 and Figure 4-8 show the time histories of the input motion in *X* direction and *Y* direction, respectively.

Figure 4-6 Tested building model

Table 4-2 Input plan[12]

Input no.	Scale	Maximum acceleration (m/s^2)		
		X	*Y*	*Z*
1	5%	0.307	0.469	0.191
2	10%	0.785	0.916	0.391
3	25%	1.97	2.99	0.946
4	50%	3.43	4.74	1.86
5	100%	6.30	11.40	3.45
6	60%	3.11	5.40	1.93

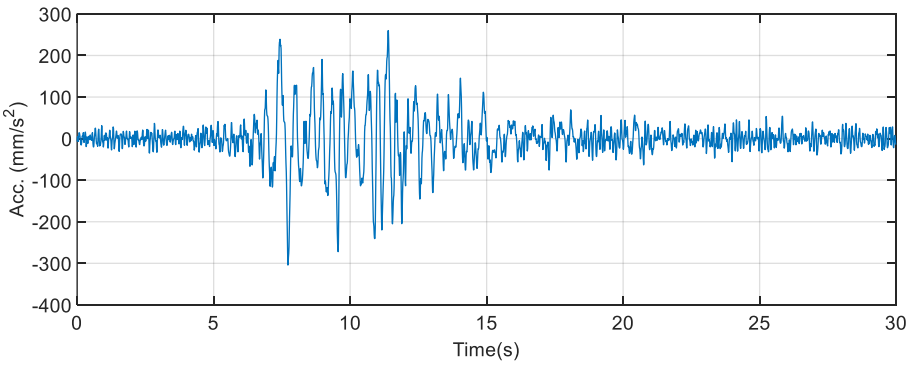

(a) Input 1

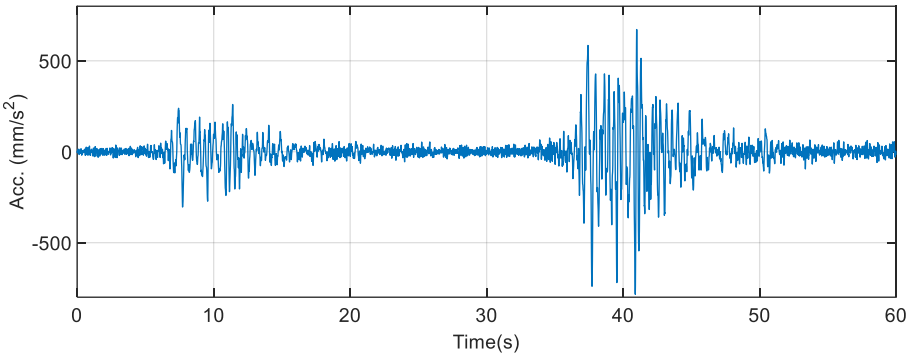

(b) Input 2

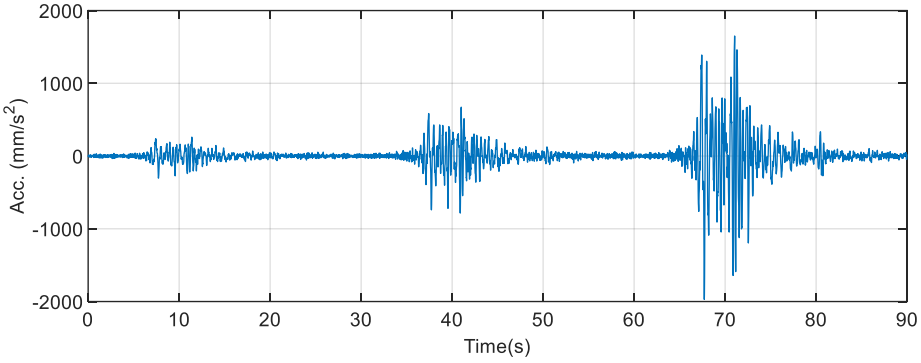

(c) Input 3

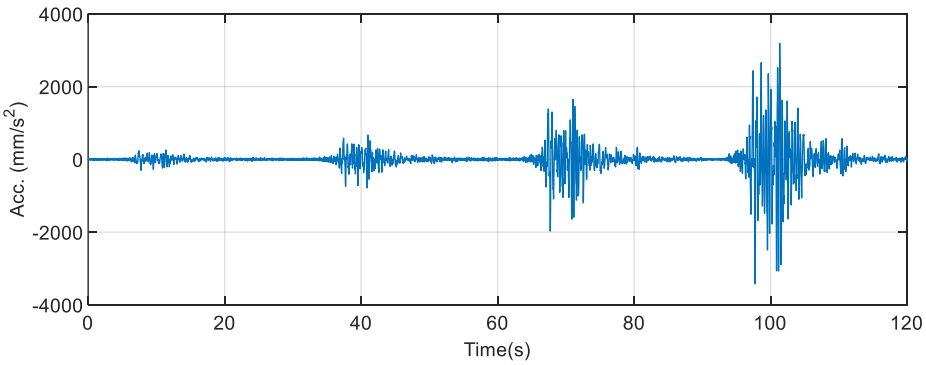

(d) Input 4

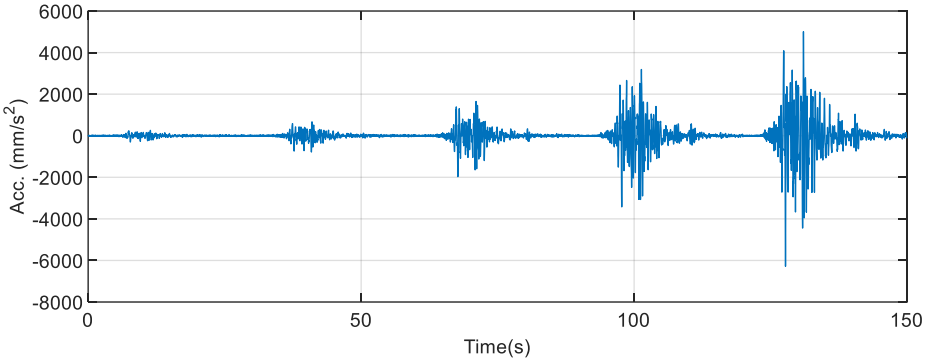

(e) Input 5

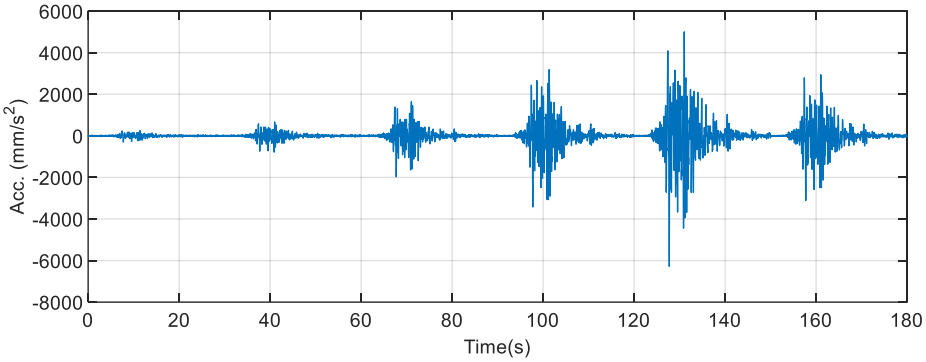

(f) Input 6

Figure 4-7 Time histories of input motion in *X* direction

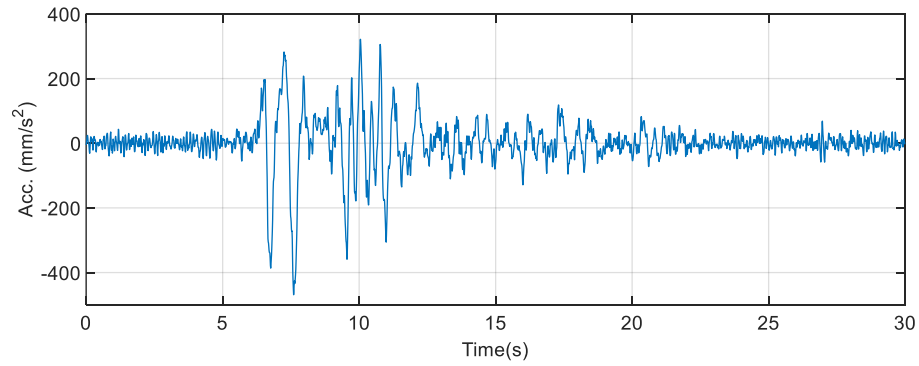

(a) Input 1

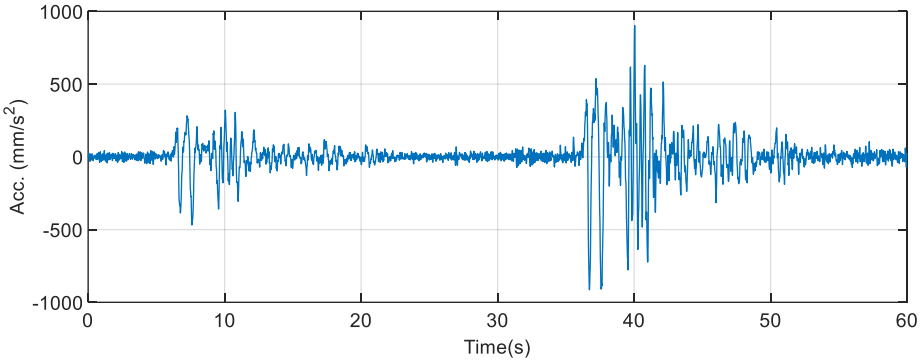

(b) Input 2

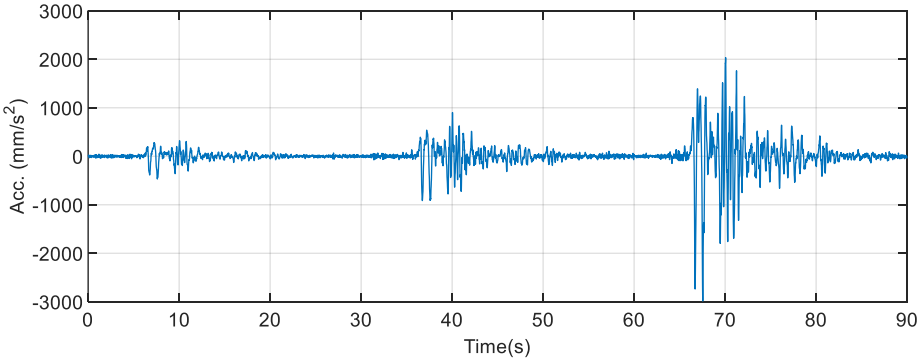

(c) Input 3

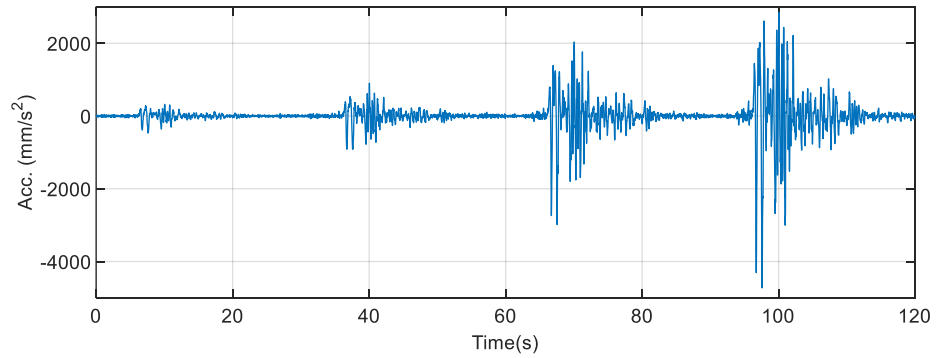

(d) Input 4

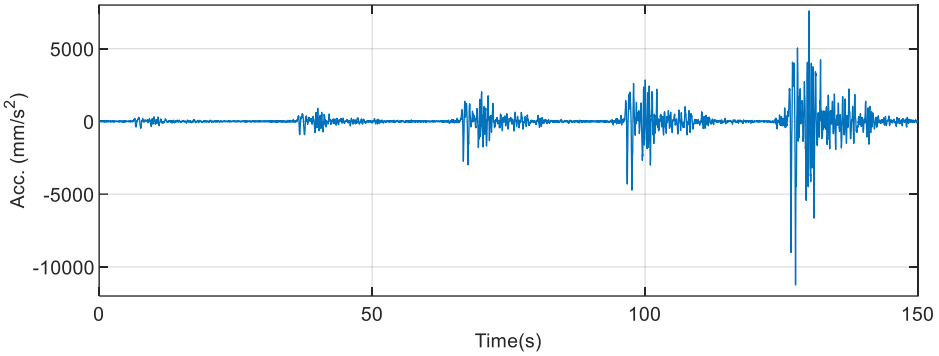

(e) Input 5

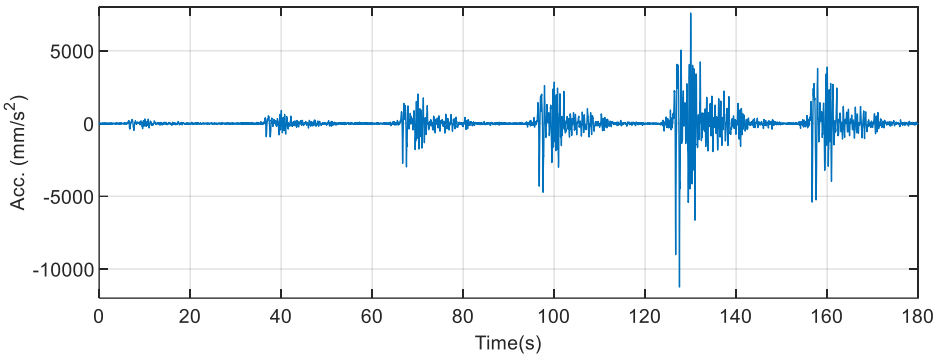

(f) Input 6

Figure 4-8 Time histories of input motion in *Y* direction

Table 4-3 Damage observation and quantification results during different cases[13]

Input no.	Test result and damage observation	Maximum deformation for the 2nd floor	
		x direction	y direction
1	Elastic behavior without damage	0.69 mm (1/3600)	0.46 mm (1/5400)
2	Flexural cracks were found on the bottom of the columns on the 1st floor	2.44 mm (1/1000)	1.32 mm (1/1900)
3	Flexural cracks were found on the end of the beams on every floor	5.19 mm (1/480)	3.96 mm (1/630)
4	Shear cracks were found on the shear wall on the 1st floor	11.15 mm (1/220)	9.22 mm (1/270)
5	Short columns and the bottom of the shear wall on the first floor suffered shear failure	48.00 mm (1/52)	98.33 mm (1/25)
6	Long columns on the 1st floor suffered compression failure; The structure was on the state of near-collapse	44.03 mm (1/57)	150.06 mm (1/17)

The capacity curve and the modeled restoring force in terms of spectral displacement and spectral acceleration were estimated for the six test cases, as shown in Figure 4-9 and Figure 4-10. In general, the capacity curves were satisfactorily correlated with the observed damage scenarios of the specimen shown in Table 4-3. In the context of spectral

displacements, one could find that values in the *Y* direction and *X* direction are almost identical for the first four input cases. However, the spectral displacements in the *Y* direction is two times larger than those in the *X* direction for the case of Input 5 and Input 6, which is consistent with observed inter-story drift angle. As illustrated by Figure 4-9 and Figure 4-10, for the case of Input 1 to 3, the capacity curve is linear or nearly linear, which agrees well with the observation that the structure was undamaged or only formed flexural cracks. The structure behaved nonlinearly in the case of Input 4 in *X* direction, as illustrated by Figure 4-9 (d), and deformed in a large nonlinear range for the Input 5. In the case of Input 5, the spectral acceleration increases with increased spectral displacement and then begin to decrease after it reaches the ultimate point. This phenomenon may be contributed to shear failure of the short columns and the bottom of the shear wall on the first floor (Figure 4-11).

Next, the damage evaluation result based on capacity curve method and post-earthquake damage evaluation guideline [13] are listed in Table 4-4 for comparison. It is shown in Table 4-4 that the result of the CCB method agrees approximately with the guideline's one, although differences can be found for the Input 4 and 5. Note that while the CCB method evaluates the damage according to the overall structural performance and the inter-story-drift-based safety limit, the guideline method requires the identification of damage state of each lateral-load resisting member and classifies the damage level based on the weighted arithmetic mean value of the damage states of members by visual inspection[1], which could lead to the differences in the assessment result. In view of this, the agreement between the guideline and the CCB method is acceptable.

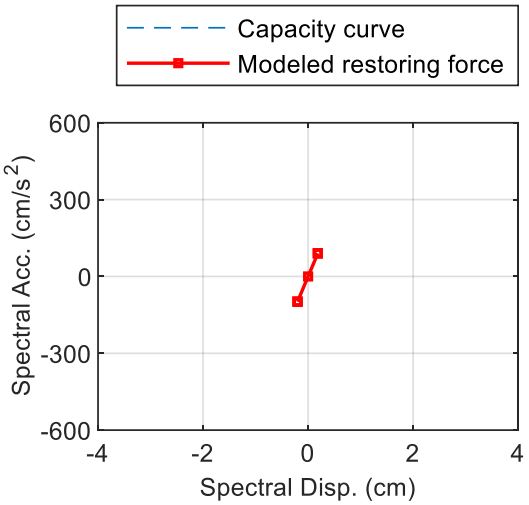

(a) Input 1

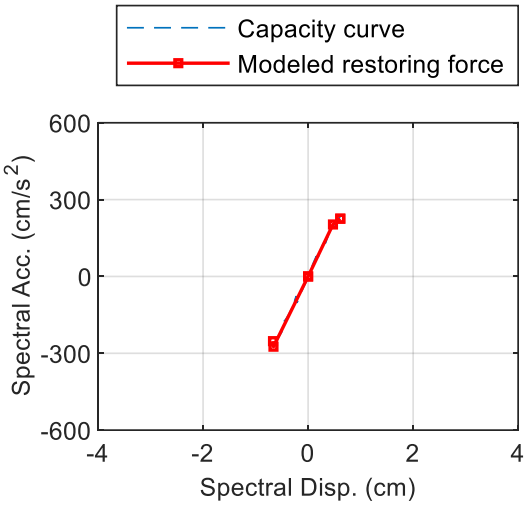

(b) Input 2

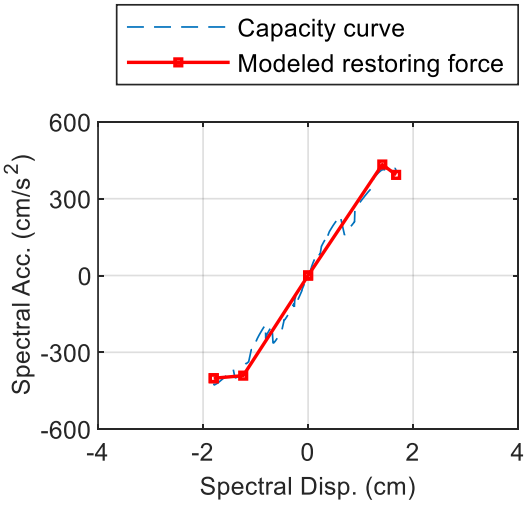

(c) Input 3

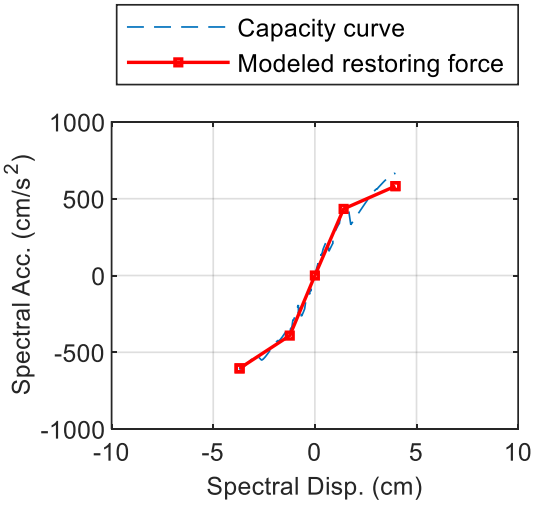

(d) Input 4

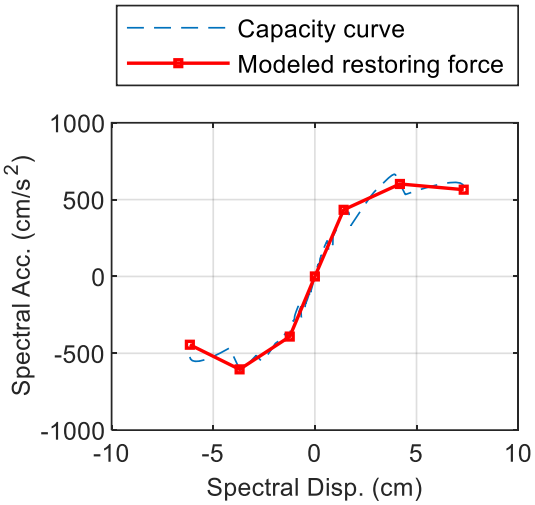

(e) Input 5

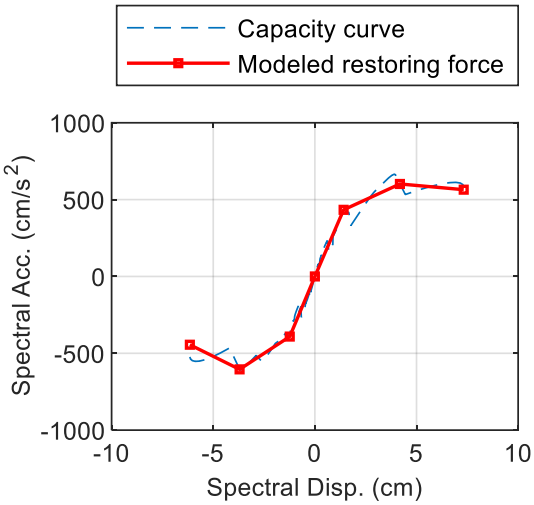

(f) Input 6

Figure 4-9 Capacity curve and modeled restoring force in X direction

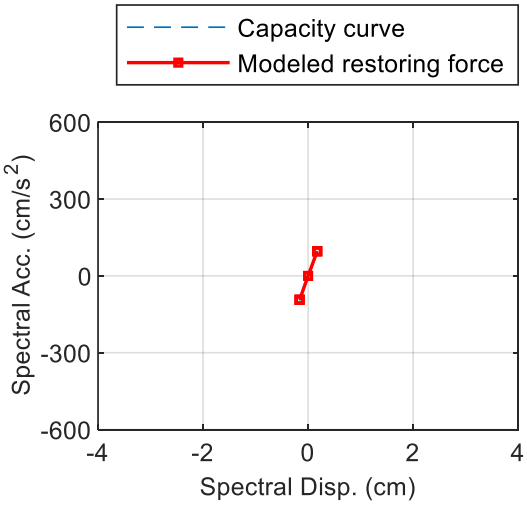

(a) Input 1

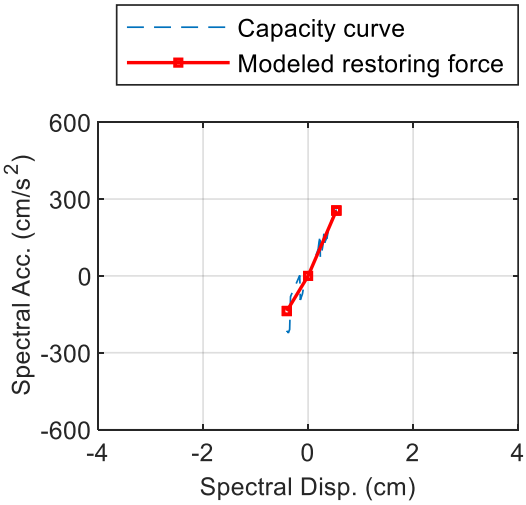

(b) Input 2

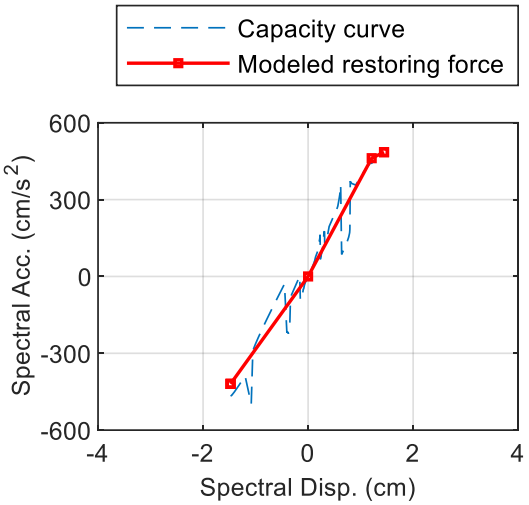

(c) Input 3

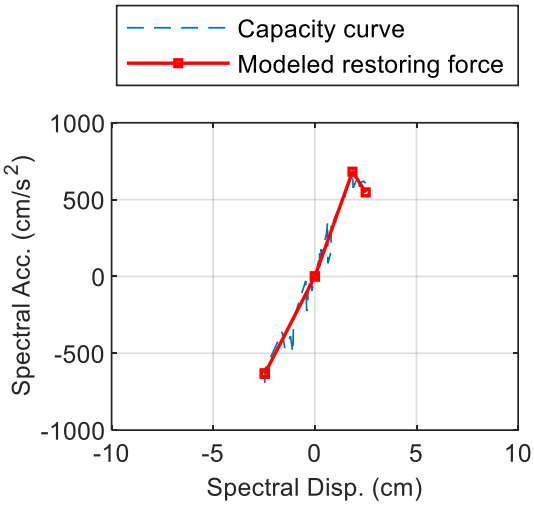

(d) Input 4

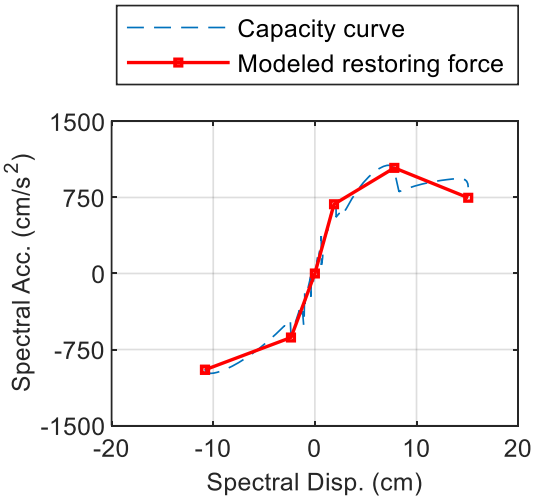

(e) Input 5

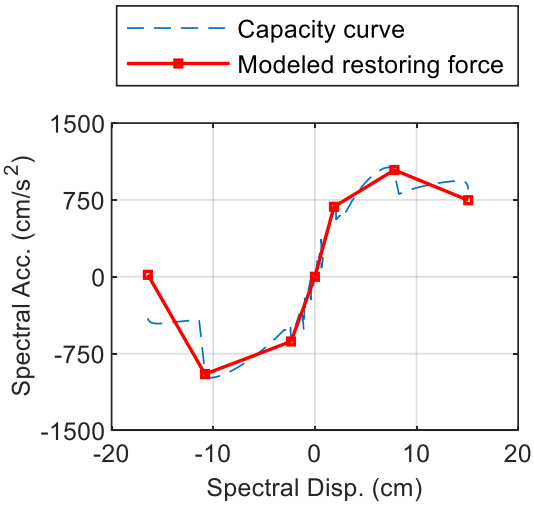

(f) Input 6

Figure 4-10 Capacity curve and modeled restoring force in Y direction

(a)

(b)

(c)

Figure 4-11 Visual inspection of damage after Input 5 (a) short column on the first floor (b) another short column on the first floor (c) shear wall on the first floor

Table 4-4 Comparison between results of CCB method and guideline

Input no.	Damage class by guideline	Damage class by the capacity curve method	
		X direction	*Y* direction
1	0	0	0
2	I	I	0
3	I	I	I
4	II	I	I
5	IV	V	V
6	V	V	V

4.4.3 Numerical investigation

The numerical model is a 2-dimension RC frame structure with 6 stories and 2 bays (Figure 4-12). The numerical simulation was performed by Open System for Earthquake Engineering Simulation (OPENSEES). To compare the result using the CCB method and the one that using Japanese guideline which evaluates the damage based on the vertical members, the RC beams were assumed to be elastic, while the columns considered nonlinear flexural characteristics to concentrate the damage in the columns during the simulation.

Table 4-5, Table 4-6 and Table 4-7 show the information on the columns and the material parameters of the reinforcement and concrete. Figure 4-14 and Figure 4-15 show the hysteretic behaviors of the steel and concrete, respectively. The ground motion used in this investigation was the seismic wave MYG013NS observed by K-NET in Sendai on March 11, 2011. which was selected as the mainshock of the MA sequence. The aftershock was then assumed to be identical as the first motion. Figure 4-13 gives the time history of the MA sequence at 100% shaking intensity.

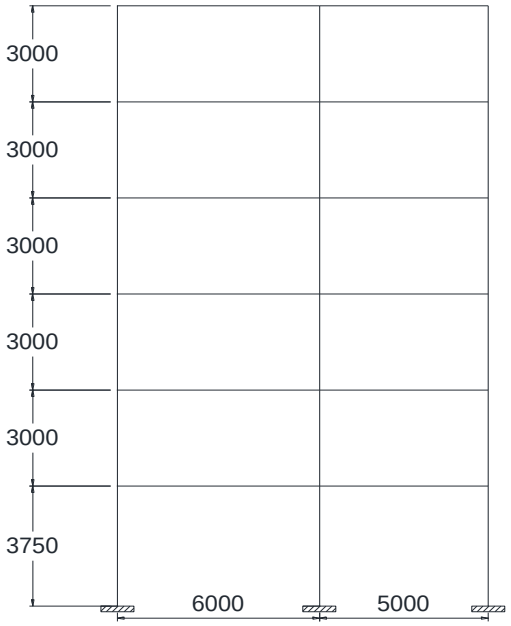

Figure 4-12 Elevation of the numerical model (unit:mm)

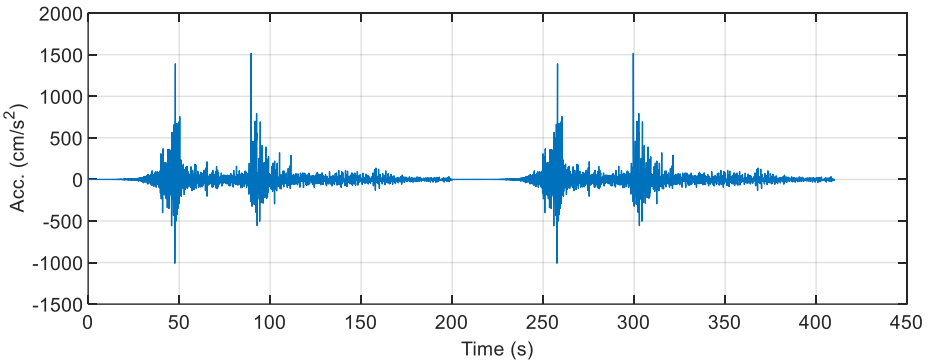

Figure 4-13 Time history of MA sequence at 100% shaking intensity

Table 4-5 Details of the columns

	Dimension (mm×mm)	Longitudinal reinforcement (mm^2)
Column	500×500	3040

Table 4-6 Mechanical properties of the reinforcement

Material	Yield strength (N/mm^2)	Initial elastic tangent (N/mm^2)	Strain-hardening ratio
Steel	345	2×10^5	0.02

Table 4-7 Mechanical properties of the concrete

Material	Compressive strength (N/mm^2)	Strain at maximum strength	Crushing strength (N/mm^2)	Strain at crushing strength
Concrete	30	0.002	15	0.003

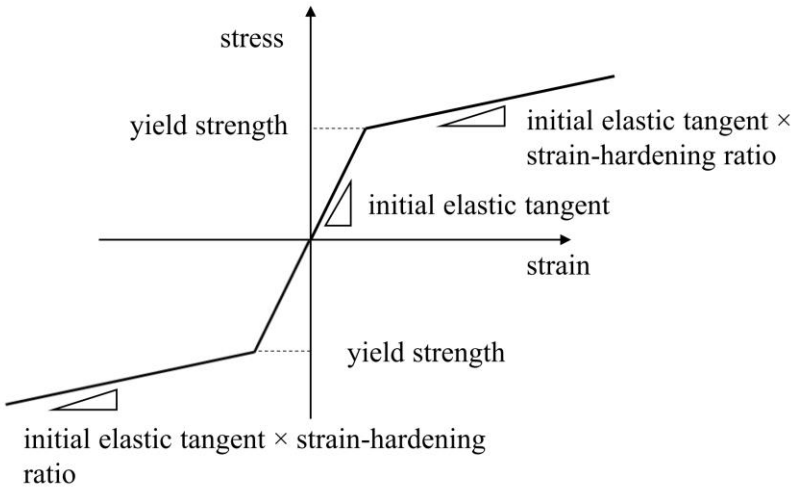

Figure 4-14 Hysteretic behavior of steel

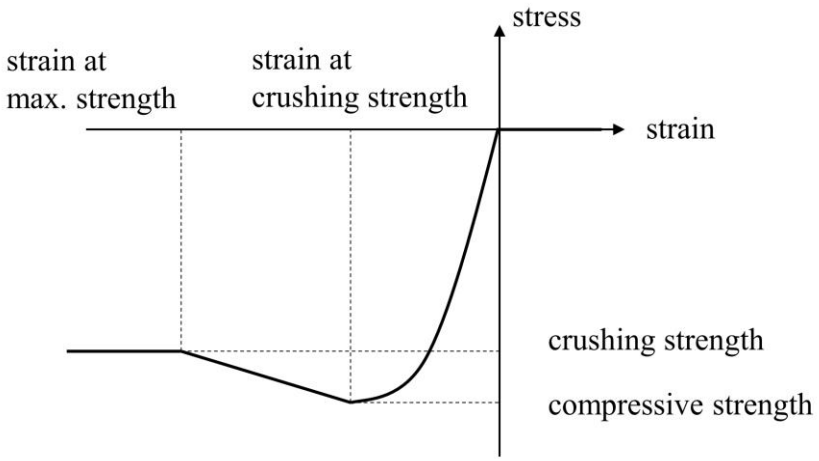

Figure 4-15 Hysteretic behavior of concrete

The input motion was scaled to different levels of peak ground motion so that the building could deform from the linear-elastic range to the nonlinear range. Accelerations at each floor were simulated by the time history analysis of the building model subjected to the ground motion at the base of the building. Figure 4-16 gives the high-wise distribution of the maximum story drift angle of the building under various levels of the MA sequence. The increasing responses caused by the increasing intensity of the input motions are apparent in the figure. The largest story drift angle occurred at the bottom floor and increased sharply after 20% intensity, which indicates the bottom floor had deformed into nonlinear range. Meanwhile, the drift angles at other floors were small and grew gradually with increasing intensity.

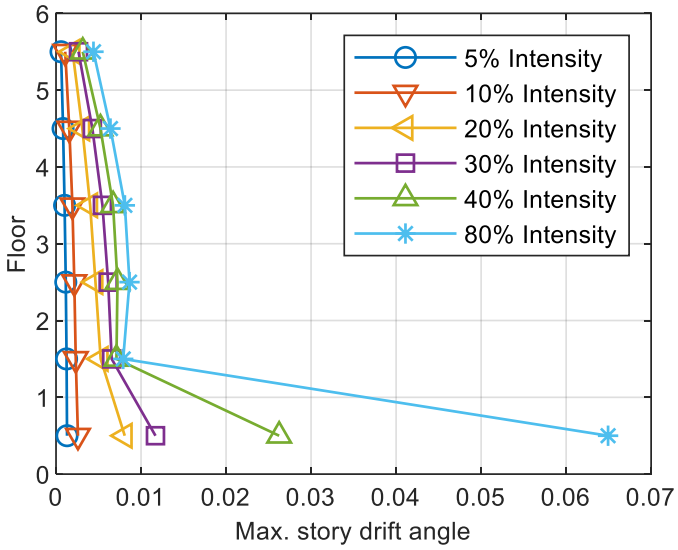

Figure 4-16 High-wise distribution of the maximum story drift angle

Using the recorded floor accelerations and ground motion during the mainshock of the MA sequence, the capacity curve and demand curve of each seismic events are estimated. For the input at 5% and 10% shaking intensity, the structure behaves within the elastic range, as shown by the linear capacity curve in Figure 4-17 (a) and (b). The capacity curve intersects the 5% elastic demand curve in its linear-elastic region, indicating that the structure would behave linearly after the excitation of the aftershock. The structure initiated nonlinearity under the input at 20% intensity, and nonlinearity increased with increased input motion. Therefore, the demand curves from input at 20% intensity to 80% intensity are reduced from the 5% elastic demand curve. As shown in Figure 4-17 (c)-(f), the intersection point tends to be closer to the preset safety limit (SL) as the excitation increases, which means the damage class for aftershock is getting higher. Note that the maximum deformation points lie beyond the SL under the input at 80% intensity. This indicates the structure has already collapsed during the mainshock.

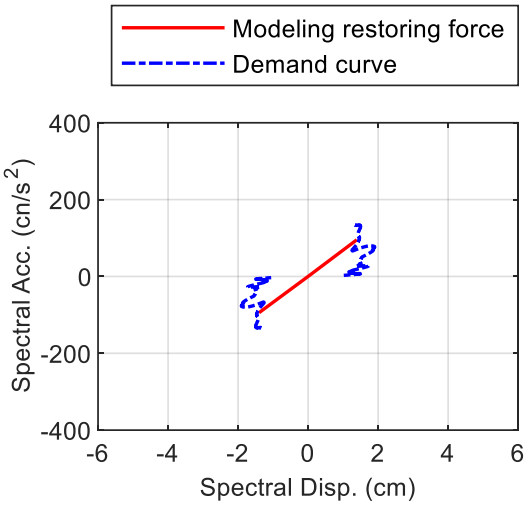

(a) 5% intensity

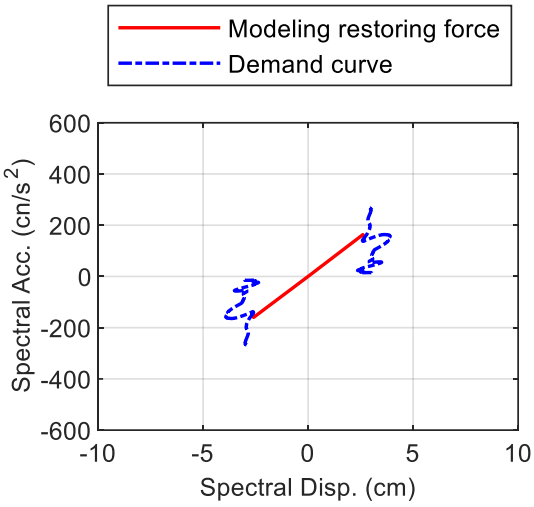

(b) 10% intensity

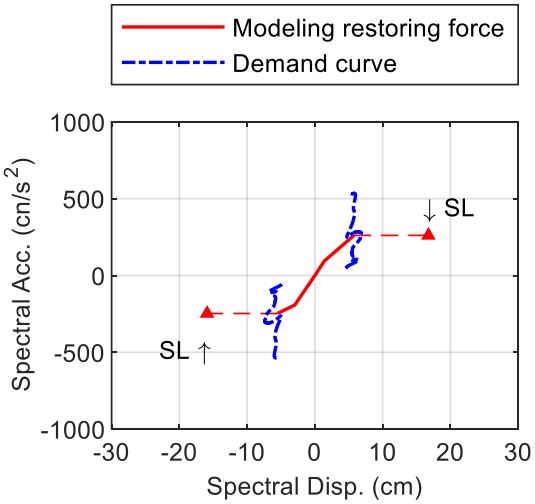

(c) 20% intensity

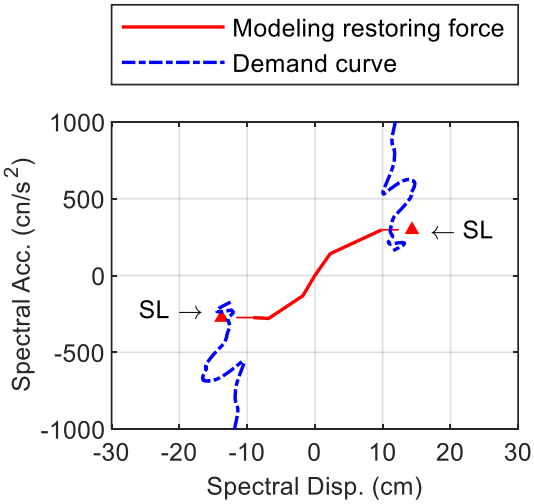

(d) 30% intensity

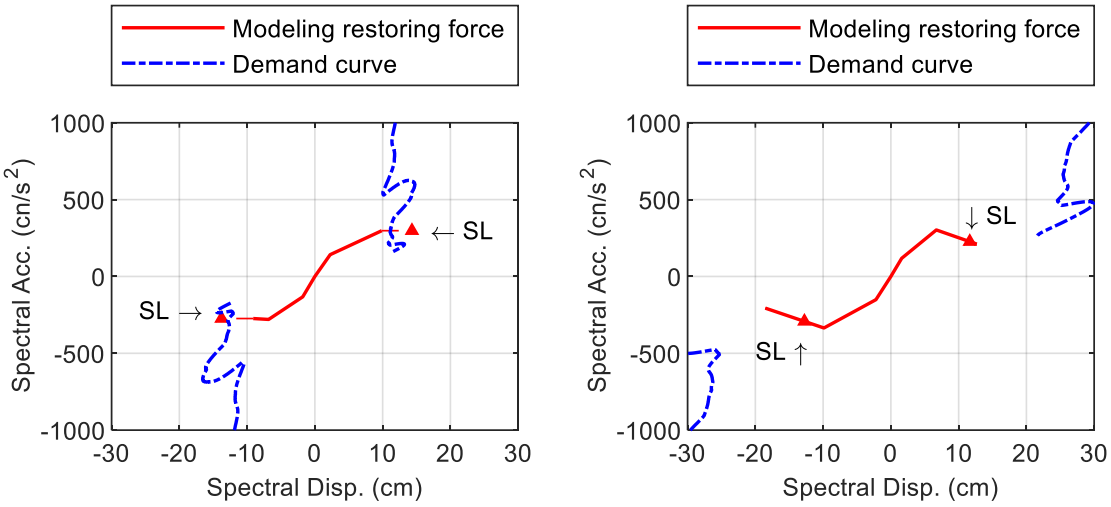

(e) 40% intensity (f) 80% intensity

Figure 4-17 Capacity curve and demand curve

The predicted aftershock damage class using the proposed method would be compared with the one using the guideline method in Japan. Since visual inspections are not available in this case, the damage class of the structure would be determined based on the ratio of the residual energy dissipation capacity to the original energy dissipation capacity of the member. A summary of the procedure for damage evaluation using guideline is given here.

1. Adjust the MA sequence to the same intensities in the experimental studies and perform structural analysis to obtain the maximum axial forces and maximum curvatures of the bottom and the top section of the columns.
2. Perform sectional analysis to obtain the moment-curvature behavior for the bottom and top sections of each member under the obtained axial forces in step 1. The ultimate limits of the curvatures of the sections are set where the strain at the extreme compression fiber of the concrete reaches 0.0033.

3. The obtained moment-curvature curves from step 3 is first converted a trilinear fitting curve. Next, with the modeled curve and the maximum curvature predicted from structural analysis in step 1, the η parameter is calculated, according to the definition in Figure 6. To estimate post-yield scant unloading stiffness for the trilinear model, the stiffness degradation factor adopted here is 0.4.
4. Select the smallest η considering both the top and bottom sections of each column and calculate the *R* of each floor using Eq. (4-3). The smallest *R* overall represents the damage condition of the entire structure.

The damage evaluation result based on capacity curve method and post-earthquake damage evaluation guideline are listed in Table 4-8. It is shown that the result of the proposed method agrees fairly well with the guideline's one, although in the moderate damage and severe damage condition, the damage class for the guideline are higher. The major reason for these differences may due to the damage classes defined in these two methods. For the proposed method, the region between Class II to Class IV is divided evenly in terms of the entire structure capacity curve. On the other hand, in the guideline, the region between Class II to Class IV is split in terms of dissipated energy ratio of each members and then take the average of damage classes of the members as an indicator for the overall damage condition.

Table 4-8 damage evaluation results for aftershock

Input level	Scale	Damage evaluation result	
		Capacity curve method	Japanese guideline
		Damage class	
1	5%	0	I
2	10%	I	I
3	20%	III	III
4	30%	III	IV
5	40%	IV	V
6	80%	V	V

4.5. Conclusions

Validation of post-earthquake damage evaluation was presented and the results using the capacity curve method was compared with those using guideline in Japan. First, field survey results and an experimental investigation of a 6-story RC building model using the CCB damage evaluation method are demonstrated. The results of CCB method agree fairly well with the visual inspection's one. Next, the capacity curve method for aftershock damage prediction is validated by the simulated data from a 6-story RC frame structure under earthquakes and comparisons with guideline are made, which also shows good agreement.

4.6. References

[1] Maeda, Masaki, and Dae Eon Kang. "Post-earthquake damage evaluation of reinforced concrete buildings." *Journal of Advanced Concrete Technology* 7, no. 3 (2009): 327-335.

[2] Kusunoki, “Development of Building Monitoring System to Evaluate Residual Seismic Capacity after an Earthquake.” *News Letter Plus, Earthquake Research Institute, The University of Tokyo,* no.29 (2018)

[3] Kusunoki, Koichi, et al. "A new method for evaluating the real-time residual seismic capacity of existing structures using accelerometers: Structures with multiple degrees of freedom." *Japan Architectural Review* 1.1 (2018): 77-86.

[4] Midorikawa, Mistumasa, et al. "Performance-based seismic design code for buildings in Japan." *Earthquake Engineering and Engineering Seismology* 4.1 (2003): 15-25.

[5] Ministry of Land, Infrastructure, Transport and Tourism, Notification No. 1457-6: *Technical Standard for Structural Calculation of Response and Limit Strength of Buildings*, 2000. (In Japanese)

[6] Kusunoki, K and Teshigawara M. “Numerical study for estimating the substitute damping coefficient for an aftershock.” *Proceedings of the Japan Concrete Institute*. 28.2 (2006):1057-1062 (In Japanese)

[7] Kusunoki, K.“Analytical study on the prediction method of the safety limit deformation on the performance curve by using measured data during an earthquake ” *Journal of Structural and Construction Engineering* (Transactions of AIJ) (2019)(accepted, In Japanese)

[8] Vamvatsikos, Dimitrios, and C. Allin Cornell. "Direct estimation of seismic demand and capacity of multidegree-of-freedom systems through incremental dynamic analysis of single degree of freedom approximation." *Journal of Structural Engineering* 131.4 (2005): 589-599.

[9] Shi, Wei, et al. "Development of seismic collapse capacity spectra and parametric study." Advances in Structural Engineering 17.9 (2014): 1241-1255.

[10] Xiong, Chen, et al. "A nonlinear computational model for regional seismic simulation of tall buildings." *Bulletin of Earthquake Engineering* 14.4 (2016): 1047-1069.

[11] Xiong, Chen, et al. "Parameter determination and damage assessment for THA-based regional seismic damage prediction of multi-story buildings." *Journal of Earthquake Engineering* 21.3 (2017): 461-485.

[12] Kim, Yousok, Toshimi Kabeyasawa, Taizo Matsumori, and Toshikazu Kabeyasawa. "Numerical study of a full-scale six-story reinforced concrete wall-frame structure tested at E-Defense." *Earthquake Engineering & Structural Dynamics* 41, no. 8 (2012): 1217-1239.

[13] Matsumori T, Shirai K, Kabeyasawa T. “Study on seismic performance of R/C wall-frame structures based on large-scale shaking table test: outline offull-scale 6-story specimen and tri-axial shaking table test.”*Journal of Structural Construction Engineering* (Transactions of AIJ). 2007;72:85-90. (in Japanese)

Chapter 5. Conclusions and future work

5.1. Conclusions

A rapid and reliable methodology for estimating capacity curve using wavelet transform for damage evaluation with limited number of accelerometers was proposed and a validation of the CCB method was presented in this study.

In **Chapter 2**, a novel procedure for deriving structural capacity curve from its earthquake acceleration response was presented. A clear advantage of this method is that it frees one from choosing cutoff frequencies manually and is capable of generation of capacity curve in a relatively short time. Structural damage or a change in system stiffness can be well displayed through a simplified force-displacement relationship. The feasibility of the proposed method is demonstrated by numerical examples, shaking table tests and actual recorded data of a steel tower during an earthquake event.

In **Chapter 3**, a strategy for capacity curve estimation from accelerations at limited floors is proposed. Numerical simulations and shaking table tests have shown that the estimations based on the PWCPI procedure using data from sensors placed at regular intervals provide good estimates at the linear-elastic range as well as the nonlinear range. The entire procedure does not require sensors to be installed at optimal locations calculated from the modal property. This finding is useful and convenient in practice, because modal property, such as mode shape, is not always available for the instrumented building. The required number of sensors is also provided in this study.

In **Chapter 4**, validations using field survey results, shaking table tests and numerical simulations are presented and comparison between the capacity-curve-based method and

code-specified visual inspection method are made. It is shown that the damage evaluation results using the CCB method agree fairly well with those of visual inspection during the tests, indicating that the CCB method could serve as a useful tool for post-earthquake damage evaluation.

5.2. Future work

- The long-period component in the measured signal eliminated by WTM may lead to the elimination of residual displacement after applying double integration. Thus, the maximum displacement of derived capacity curve could be less than the actual value when the structure subjected to large inelastic deformations during violent ground motion. In this case, it may be possible to model the restoring force of the capacity curve from the acceleration measurement value and then extract the residual deformation component by WTM from the result of the elastoplastic analysis using this restoring force model. Next, by adding the extracted residual deformation component to the displacement calculated by double integral of the measured accelerations, the capacity curve in consideration of the residual deformation can be obtained. In addition, global positioning system (GPS) could be an alternative. In recent years, the improvement of GPS has allowed near real time (100 Hz) positioning with the accuracy in the order of millimeter to centimeter. In this regard, it may be possible to recover the residual displacements using the GPS technology in future studies.
- The original formulation of the capacity curve method is based on the fundamental mode of vibration, and higher mode effects are neglected in this study for damage evaluation. Extensions that account for higher mode effects for the capacity curve

has been studied in previous studies and its application on the damage evaluation could be considered in future studies.

- Regarding the sensors placement, further research is needed for buildings where stiffness changes significantly, such as irregular unsymmetrical buildings and buildings with soft story. For this kind of buildings, additional sensors may be needed for interpolations to estimate the capacity curve.
- This study for damage evaluation has a narrow focus on RC structures, because they are widely constructed around the world. Extensions to other kinds of structure system, such as timber houses and steel structures, may be carried out in the future.

5.3. Publications

Journal papers

[1] **H Pan**, K Kusunoki. A wavelet transform based capacity curve estimation approach using seismic response data. *Structural control and health monitoring*. 2018, 25(12):e2267. (SCI, JCR Q1)

[2] **H Pan**, K Kusunoki. Capacity curve estimation for high-rise buildings using limited numbers of sensors. *Journal of earthquake engineering*. 2019 (In press DOI: 10.1080/13632469.2019.1592792) (SCI, JCR Q1)

[3] **H Pan**, K Kusunoki, Y Hattori. A capacity curve-based damage evaluation approach for reinforced concrete buildings using seismic response data. *Engineering structures* (Accepted) (SCI, JCR Q1)

[4] **H Pan**, K Kusunoki. Aftershock damage prediction for reinforced concrete buildings using recorded seismic response from mainshock *Soil dynamics and earthquake engineering* (Minor revised, resubmitted) (SCI, JCR Q2)

[5] **H Pan**, K Kusunoki, M Yamazoe and Y Sako. Large scale shaking table tests on a three-story reinforced concrete building sitting on pile foundations *Earthquake engineering and structural dynamics* (In review) (SCI, JCR Q1)

Conference papers

[1] **H Pan**, K Kusunoki. PWCPI-based procedure to estimate capacity curve for instrumented high-rise buildings. *The Pacific Conference on Earthquake Engineering and annual New Zealand Society for Earthquake Engineering conference. Auckland, New Zealand*, 2019

[2] **H Pan**, K Kusunoki. Damage evaluation for RC buildings using seismic response data *The 7th world Conference of Structural Control and Monitoring. Qingdao, China,* 2018

[3] **H Pan**, K Kusunoki. Damage evaluation for RC buildings using seismic response data. *Summaries of technical papers of Annual Meeting Architectural Institute of Japan. Structures I*. Sendai, Japan, 2018

[4] **H Pan**, K Kusunoki. Full scale monitoring of typhoon effects on a super tall building. *Summaries of technical papers of Annual Meeting Architectural Institute of Japan. Structures I*. Hiroshima, Japan, 2017